INTERNATIONAL ATOMIC ENERGY AGENCY
UNITED NATIONS EDUCATIONAL, SCIENTIFIC AND CULTURAL ORGANIZATION

INTERNATIONAL CENTRE FOR THEORETICAL PHYSICS
34100 TRIESTE (ITALY) - P.O.B. 586 - MIRAMARE - STRADA COSTIERA 11 - TELEPHONE: 2240-1
CABLE: CENTRATOM - TELEX 460392-I

H4.SMR/286 - 13

SECOND WORKSHOP ON

OPTICAL FIBRE COMMUNICATION

(14 - 25 March 1988)

SOURCE COUPLING, SPLICES, CONNECTORS AND PASSIVE DEVICES

S. Celaschi
CPQD/TELEBRAS
CAMPINAS, BRASIL

LECTURES AT ICTP

MAIN TITLE: SOURCE COUPLING, SPLICES, CONNECTORS AND PASSIVE DEVICES

1ST LECTURE: - INTRODUCTION
- SOURCE COUPLING
- SPLICES AND CONNECTORS

2ND LECTURE: - POLISHED COUPLERS
- FUSED COUPLERS

3RD LECTURE: - TUNABLE LIGHT SPLITTERS AND ATTENUATORS

DR. SERGIO CELASCHI

MARCH 1988 - TRIESTE

SOURCE COUPLING, SPLICES AND CONNECTORS

INTRODUCTION

The proper design of an optical communication system using optical fibers as the transmission medium requires a knowledge of the transmission characteristics of the optical sources, fibers, and interconnection devices (connectors and splices) used to join lengths of fibers together. The purpose of this lecture is to investigate the coupling of energy from an optical source into fibers, and the effects of intrinsic and extrinsic splice-loss parameters on the transmission characteristics of an optical fiber link. In addition, examples of different types of optical fiber connectors and splices are given and the transmission loss of the interconnection devices are discussed.

SOURCE COUPLING INTO AN OPTICAL FIBER

The coupling of power from an optical source into a fiber is defined by the coupling efficiency

$$\eta = P_F / P_S \qquad (1)$$

where P_F is the power injected into the fiber core and P_S is the output power of the source. The factors affecting η can be broadly divided into two categories. The first category, loss due to unintercepted illumination, can be caused by the source's

emitting area being larger than the fiber s core area. Unfortunately, the brightness of an image on the fiber core cannot exceed that of the source and so an intermediate lens cannot focus all the ligth into the core. Even if the source is smaller than the core, you can still have problems with unintercepted illumination if separation and misalignment of the source and fiber axes allow emitted light to miss the core and become lost. Coupling loss due to unintercepted illumination can be siiminated, however, if the source-emitting area and the fiber-core area are properly matched and aligned. The second category of coupling loss that affects the efficiency of source-coupling into a fiber is due to mismatches between the source beam and fiber numerical apertures. For fiber optic communication systems two types of light sources, light-emitting diodes (LEDs) and injection laser diodes (ILDs) are typically used. To calculate the coupling loss due to numerical aperture mismatch, we must first describe the radiation characteristics of LEDs and ILDs.

The radiation pattern obtained from an edge-emitting LED is siiiptical in cross section with half-power beam divergence angles of approximately $\pm 60^{0}$ and $\pm 30^{0}$. The radiation pattern obtained from a double heterojunction laser diode is also siiiptical in cross section but narrower in beam width than an LED. For exemple, the typical half-power beam divergence of an ILD are 25% and 5% perpendicular and

parallel to the junction plane, respectively (see Fig. 1).

THEORY

COUPLING EFFICIENCY USING A CONICAL LENS

We assume a single-mode laser emitting an elliptical Gaussian beam having spot sizes a and b. The laser is located at z = 0 as seen in Fig. 2 . A single-mode fiber with a spot-size c and a thin conical lens built on its end receive the light. The lens heigth is h and the core diameter is 2W. As seen in Fig. 2 , the tip of the conical lens is located at z = H. We also assume a known relationship between W and c.

Let us calculate the evolution of the field radiated from the laser as it travels through the air, traverses the lens, and is coupled to the fundamental mode of the fiber.

The field intensity of the fundamental mode radiated by the laser into free space is, according to classical Gaussian optics theory

$$E_z = f_z \cdot g_z \tag{2}$$

where

$$f_z = \left(1 + i\,\frac{\lambda z}{\pi a^2}\right)^{-1/2} \exp\left\{-\frac{x^2}{a^2}\left[\frac{1+i\lambda z/\pi a^2}{1+(\lambda z/\pi a^2)}\right]\right\} \tag{3}$$

and λ is the free-space wavelength. The expression for g_z is obtained from (3) substituting x and a with y and b.

Using the thin-lens approximation, the conical lens is assumed to act as a phase shifter. The transmission coefficients through the lens $(x^2+y^2)^{1/2} < W$ and through the air outside the lens $(x^2+y^2)^{1/2} > W$ are

$$T_1 = \exp\left\{i\,\frac{2\pi h}{\lambda}\left[\frac{n-1}{\lambda}\,(x^2+y^2)^{-1/2} - n\right]\right\} \text{ for } (x^2+y^2)^{1/2} < W$$

$$T_2 = \exp\left\{-i\,\frac{2\pi h}{\lambda}\right\} \quad \text{for } (x^2+y^2)^{1/2} > W \tag{4}$$

where n is the core index of refraction. The field arriving at the fiber is then

$$E = E_H\,T \tag{5}$$

Since the field of the fundamental mode in the fiber in the Gaussian approximation is

$$c = \exp\left\{-\frac{x^2+y^2}{c^2}\right\} \tag{6}$$

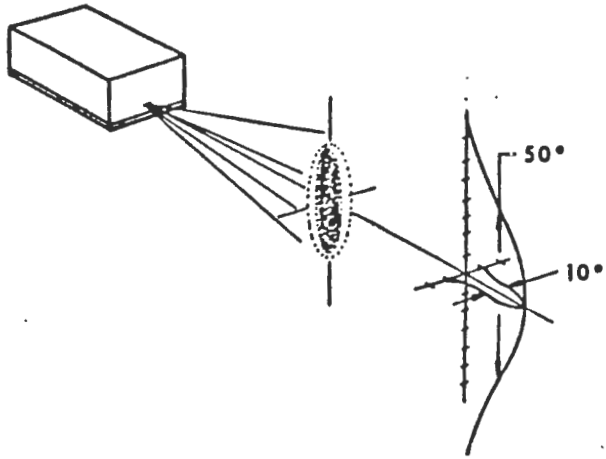

(a)

SCHEMATIC REPRESENTATION OF FAR-FIELD RADIATION PATTERN OF INJECTION LASER DIODE (ILD)

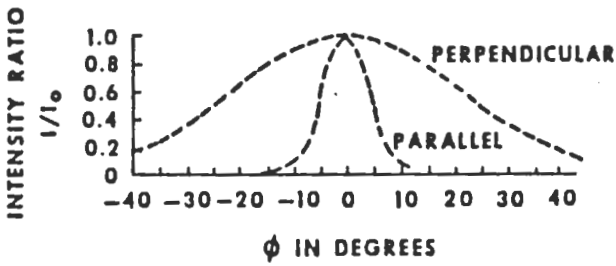

(b)

FAR-FIELD INTENSITY PATTERN OF ILD MEASURED IN PLANES PARALLEL AND PERPENDICULAR TO THE JUNCTION

FIG. 1

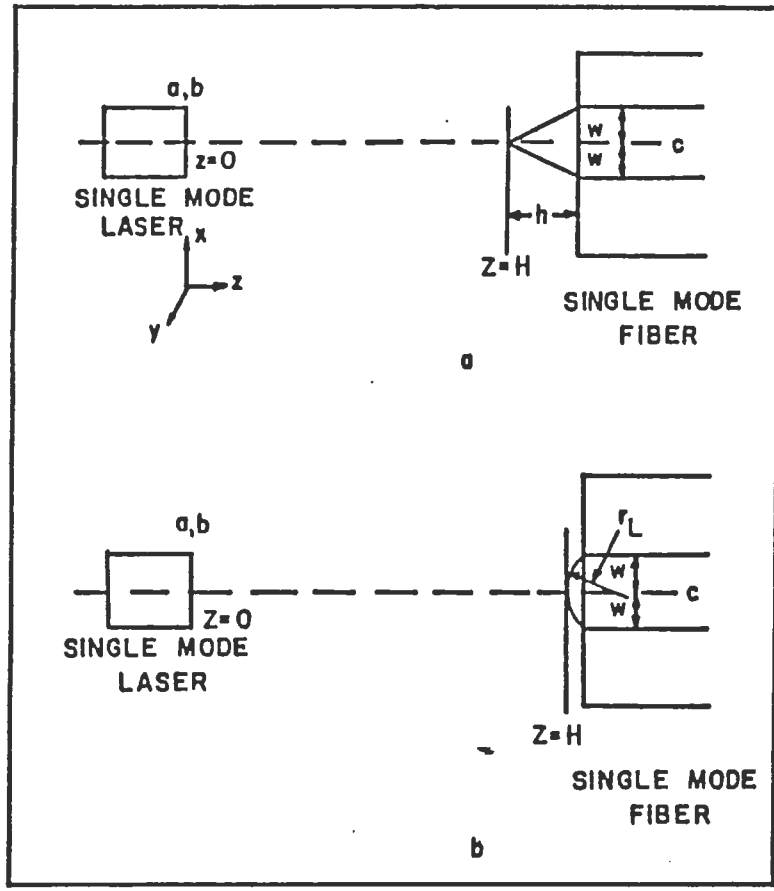

FIG. 2 - Schematics of laser to fiber coupling showing spatial parameters for (a) conical lens, and (b) hemispherical lens.

the coupling efficiency between the laser and the fiber is given by the following normalized overlap integrals:_

$$\eta = \frac{\left| \int_0^W dy \int_0^{\sqrt{W^2-y^2}} \mathcal{E}\, E_H T_1 dx \quad + \quad \int_0^\infty dy \int_{\sqrt{W^2-y^2}}^\infty \mathcal{E}\, E_H T_2 \quad dx \right|^2}{\int_0^\infty \int_0^\infty E_0^2 \, dxdy \int_0^\infty \int_0^\infty \mathcal{E}^2 \, dxdy} \tag{7}$$

The theoretical coupling efficiency for the general case of an arbitrary laser-fiber combination has been calculated including an optimization of the lens geometry (h/W) and the laser-fiber separation (H/W).

The results for a symmetrical beam are shown in Fig. 3. The optimum coupling efficiency compared with butt coupling as well as the required h/W and H/W are shown for the case of a/c = b/c ranging between 0 and 1. In Fig. 3 , c/W = 0.88 which is close to the value used in the experiments described later.

The conical lens, being circular symmetric, cannot correct for the ellipticity of a nonsymmetrical beam. In such a case, the lens can at best match the fiber spot size to the geometrical mean of the laser spot size. For nonsymmetrical beams, then, coupling efficiency is a product of two factors. The first

can be found from the η conical lenses in Fig. 3 by replacing $a/c = b/c$ by $(ab)^{1/2}/c$. Optimum lens geometry, as well as the laser-fiber separation are also determined from Fig. 3. The second factor takes into account the ellipticity of the beam and is

$$M = \frac{4ab}{(a+b)^2} \qquad (8)$$

It is plotted in Fig. 4 for ellipticity ratios a/b ranging from 0 to 1. We note that for ellipticity ratios above 0.53, M is higher than 0.9.

COUPLING EFFICIENCY USING A HEMISPHERICAL LENS WHOSE WIDTH EQUALS THE FIBER CORE DIAMETER

Such a lens may be obtained in principle by fire polishing or arc melting the etched cone. The calculation is similar to the one presented above. The conical lens is replaced by a thin hemispherical lens whose radius of curvature is r_L as seen in Fig. 2b. The calculated coupling efficiency, as well as the optimum lens geometry r_L/W and the laser-fiber separation H/W, are shown in Fig. 5 for a symmetrical beam where c/W = 0.88. To examine the increase in efficiency achieved by this

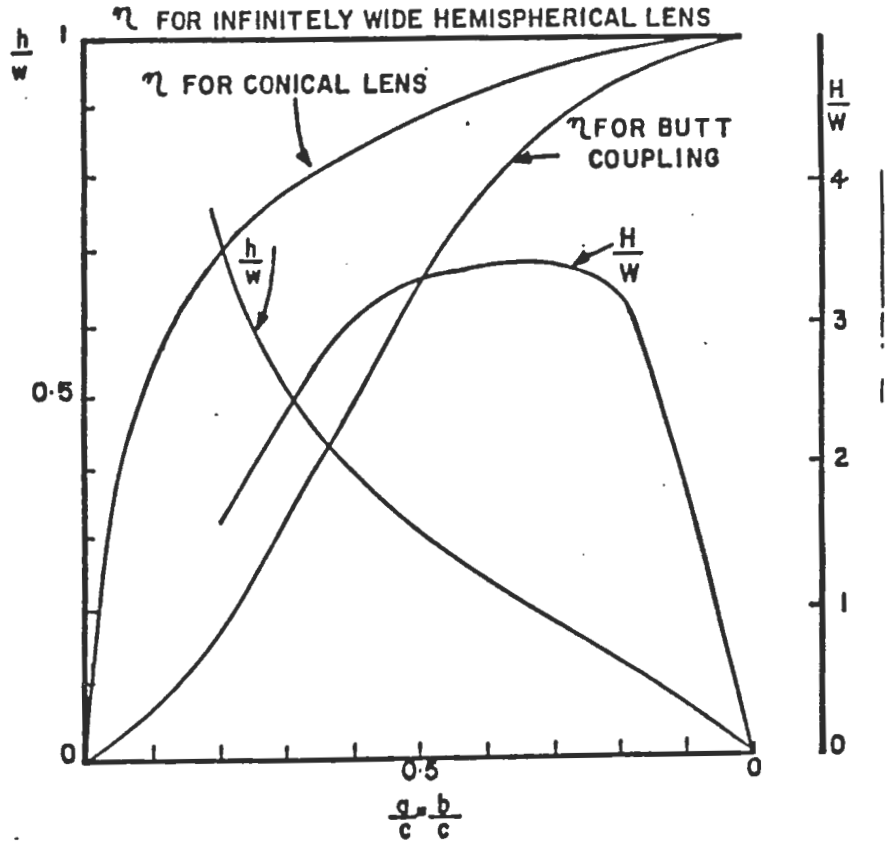

FIG. 3 - Coupling efficiency using a conical lens as a function of laser-to-fiber spot size ratio for a symmetrical beam. Optimum values for h/W and H/W are shown in the figure. Butt coupling is shown for comparison C/W = 0.88.

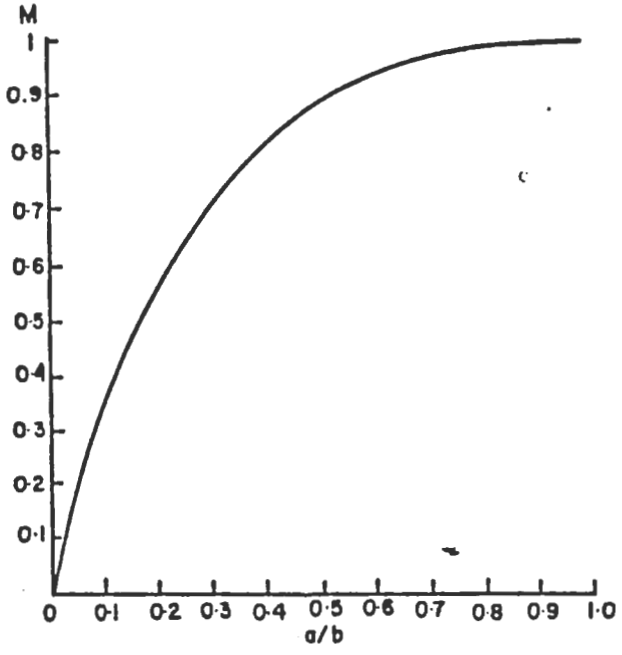

FIG. 4 - Butt coupling efficiency factor M as a function of ellipticity ratio. The geometrical mean beam spot size equals the fiber spot size.

hemispherical lens over the conical lens we compare Figs. 3 and 5 . We note that the spherical lens is more efficient, but that the increase in coupling efficiency is no more than 10% for all values of a/c = b/c.

The efficiencies presented above are different if the ratio c/W is changed. For small values of c/W the lens is effectively wide and we approach the condition of an infinitely wide lens. If c/W is large, we approach the condition of butt coupling. Maximum efficiency under both these extreme conditions is shown in Fig. 5 .

LENS MANUFACTURING

The lens is manufactured by a selective chemical etch of the fiber. It is conical in shape and may be fire polished or arc melted into a hemispherical shape. Its base always equals the fiber core diameter. This lens has two major advantages: (1)it is easy to manufacture and is reproducible: it also allows batch processing; (2) it is automatically aligned with the fiber core as seen in Fig. 6.

EXPERIMENTAL RESULTS

A 1.3 um Fujitsu double channel planar buried heterostructure laser was used in the experiments. The infared beam spot sizes were a = 0.63 um and b= 0.9 um. Hence, a/b = 0.7 and $(ab)^{1/2}/c$ = 0.17. According to Fig. 3, the calculated coupling

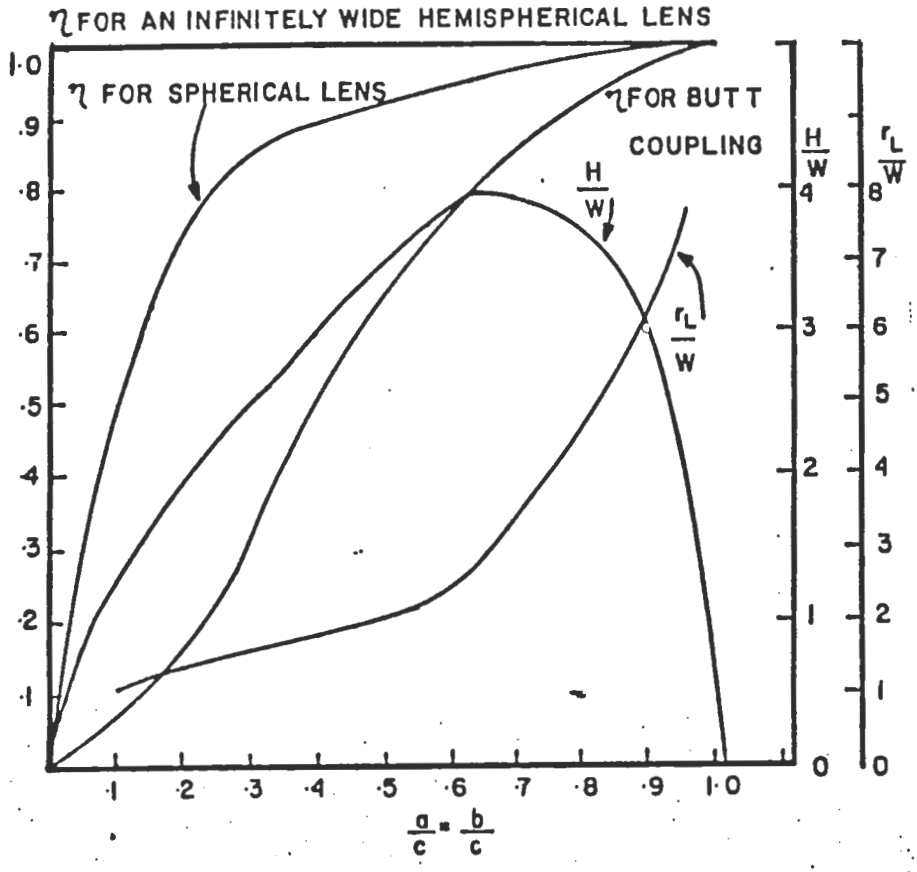

FIG. 5 - Coupling efficiency using a spherical lens as a function of laser-to-fiber spot size ratio for a symmetrical beam. Optimum values for h/W and H/W are shown. C/W = 0.88.

efficiency is approximatelly 87%. From Fig. 4, the ellipticity factor is M = 0.97, which reduces the coupling efficiency to 85%. Minimum Fresnel losses would drop this number to the level of 82%. The experimental results for the coupling efficiency are shown in Fig. 7 as a function of etching time. One can observe from the figure that the maximum coupling efficiency is around 82%. It is important to notice that maximum coupling was observed using a cone-truncated lens. Etching times longer than 2.5 hours lead to totally conical lens having coupling efficiencies of 55%. These results are predicted by the present model. Cone-truncated lens closely resembles the spherical shape, which according to the model provides better coupling to the fiber.

The calculated butt-coupling efficiency is 28%, which agrees, within the experimenatal error, to the measured value. According to Fig.3, the required lens should have h/W = 0.88 which is close to the value used in the experiment (h/W = 0.8). An optimum working value of h/W = 1.3 was set for maximum coupling which meets to the predicted ratio. The experimental c/W ratio was around 1.1, somewhat above the value used in the calculations (c/W = 0.98).

CONCLUSIONS

It is presented a theoretical design of both conical and hemispherical microlenses, whose widths coincide with the core

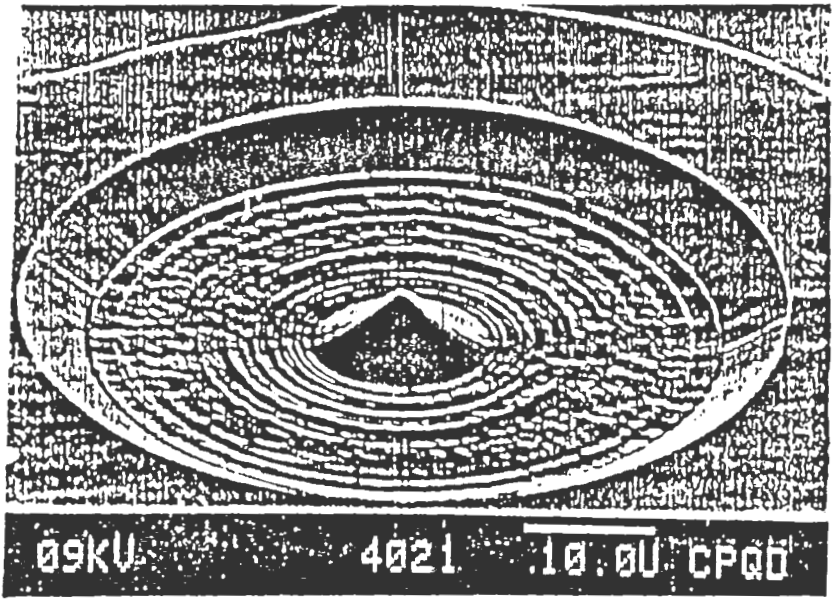

FIG. 8 - Chemically etched conical lenses on a single-mode fiber. h/W = 0.8.

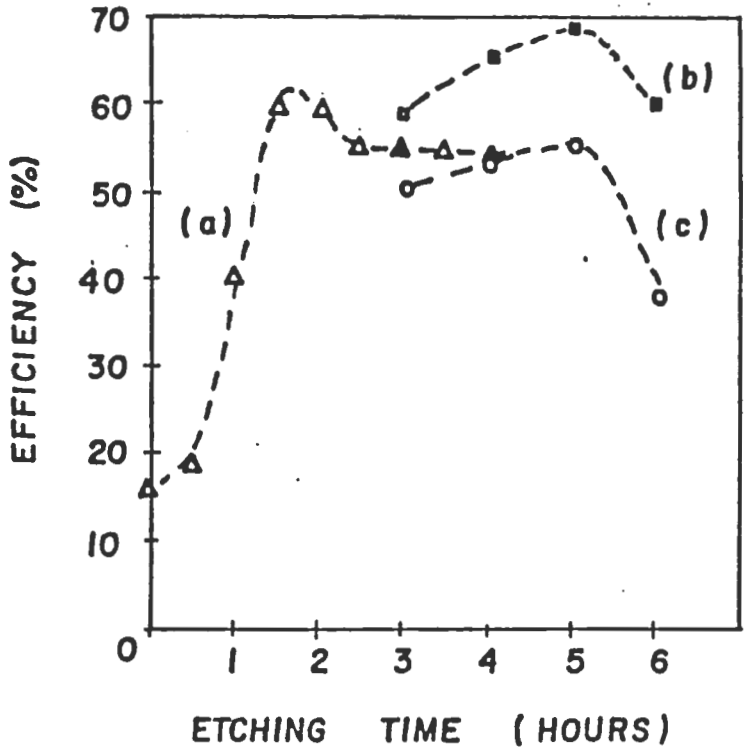

FIG. 7 - Coupling efficiencies as a function of etching time for (a) a single mode fiber, and (b) a gradual multimode fiber coupled to a ILD. The coupling efficiency observed between a MM fiber and a LED is shown by curve (c).

diameter. Maximum coupling efficiency as well as the optimum lens geometry and laser-fiber separation have been calculated for a wide range of laser beam and fiber spot sizes. Optimum separation between fiber and laser is always finite so that the use of these lenses avoids the need to bring the two into close physical proximity. We conclude that the use of these simple lenses improves the coupling efficiency in practical cases by large amounts. The experimental results presented support this conclusion.

BIBLIOGRAPHY

- Allen H.Cherin, "An Introduction to Optical Fibers", McGraw Hill, 1983.
- G.Eisenstein and D.Vitello, Applied Optics 21, 3470 (1982).
- F.F. Ildefonso and F.R.Barbosa, Private Communication.

SPLICES AND CONNECTORS

INTRODUCTION

The functions of splices and connectors are to interconnect the transmission media and to connect the media to optical devices. Splices are intended to stay permanently connected. Connectors, on the other hand, are designed for frequent separation and rejoining. The most operationally significant system parameter of these components is optical loss. The loss is dependent on alignment of the fibers, the end conditions of the fibers, and the fiber-core parameters (primarily core diameter and peak index difference in multimode fibers, and mode-field diameter in single-mode fibers). These fiber-core parameters are not under control of the splice or connector design.

The technology of lightwave system has shifted from the graded-index multimode (MM) fiber to single-mode (SM) fiber that operates at 1310 nm and/or 1550 nm in essentially all systems. The smaller core size of SM media makes splicing and connecting much more difficult. Most SM cores are about 8 um in diameter compared to 50 or 62.5 um for MM cores.

The optical loss of a splice or a connector is directly related to the accuracy of the alignment, and for a given process, the cost increases with accuracy of alignment. The cores of SM fibers must be aligned to within 1 um in a connector, with no

Fresnel reflection loss, to obtain a loss of a few tenths of a dB. Misalignment can be up to 3 um if a loss of 2 dB is allowed. The cost of the connectors tends to differ inversely by about the same ratio.

Optical-loss requirements are not the same for all applications. Low-loss components are needed for long-haul intercity trunks to get maximum spacing between regenerators. An overview of the designs and performance of splice and connectors is presented.

SPLICING

The two fundamental approaches to splicing optical fibers are fusion welding and mechanical joining. Both methods require three basic steps:

1. Fiber end preparation
2. Alignment of the fibers
3. Retention of the fibers in the aligned position.

Arc fusion is used by many for splicing optical fibers. In this method, the fiber ends are cleaved and aligned, and the ends are melted and fused to retain the alignment. In single-mode fusion, the fibers are aligned with x-y micropositioners that are driven with a feedback signal to peak the transmission of the splice. Despite automated alignment and fusion processes in the newer machines, the quality of the splices is still sensitive to

small variations in the execution of the three basic steps and to unfavorable environmental conditions. Average field-splicing times vary greatly from 15 to 40 minutes per splice, due mostly to environmental effects.

To achieve average splice losses of 0.1 to 0.25 dB with fusion in the field, resplicing is frequently required to eliminate high-loss splices. Fusion splices are physically the smallest and when properly made have extremely stable loss over a wide temperature range. Fusion splice is currently the most widely used method.

Figure 8 is a schematic diagram showing how fibers are welded together using an electric arc. Obstacles associated with fusion splicing are related to the imperfect preparation of fiber ends, the difficulties associated with prealigning the fibers to be spliced, and the tensile strength of the fused fiber. Implementing the fusion process with fibers that have imperfect ends (surface roughness, angle, or lips) can result in a distortion of the core and formation of small air bubbles. To avoid these problems, automated fusion test sets have been developed with the following features:

- an optical viewing arrangement to simplify fiber prealignment,
- a prefusion process using a low-energy arc discharge to round the fiber ends and avoid bubble formation,
- a controlled inward movement of the fibers during fusion to prevent necking at the fused joint.

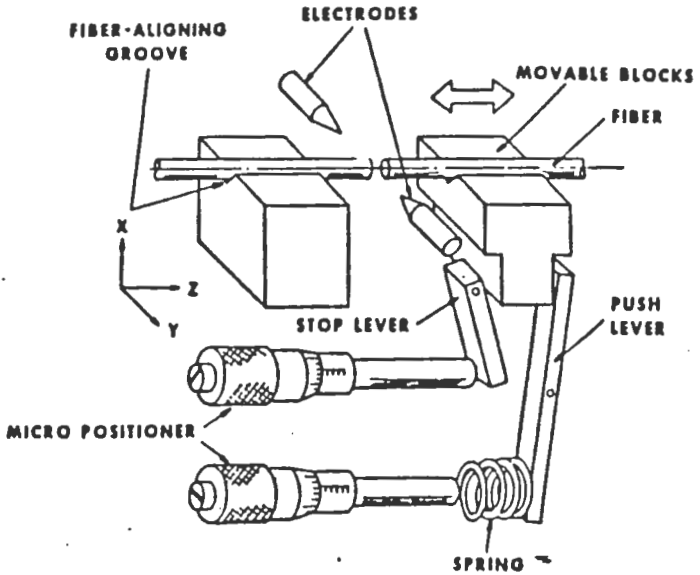

FIG. 8 - Schematic showing fusion splicing using an electric arc.

Completed fused splices should be incorporated in a protective package and stored with little or no tensile loading to avoid mechanical problems in the vicinity of the splice. Despite some of the difficulties associated with fusion splicing it is one of the most promising techniques currently available for permanently joining individual fibers.

In mechanical splices, the ground and polished ends are aligned and butted together with a matching gel or adhesive between the ends. Alignment is maintained mechanically. Some designs combine and simplify the three basic operations of end preparation, alignment, and retention to achieve increases in performance and productivity. Reflections from the fiber end faces can be made small enough that they do not interfere with the most sophisticated transmission systems by using proper index matching gels or adhesives. The remaining small reflections are an aid in analyzing faults along a fiber route with an optical time domain reflectometer.

INTRINSIC AND EXTRINSIC LOSS PARAMETERS

The losses introduced by mechanical splices and connectors are an important factor to be considered in the design of a fiber optic system since they can be a significant part of the loss budget of a multi-kilometer communication link. Losses of splices and connectors can be grouped into two categories as shown

in Fig. 8. The first category of losses is related to the technique used to join fibers and is caused by extrinsic (to the fiber) parameters such as transverse offset between the fiber cores, end separation, axial tilt, and fiber end quality. The second category of losses is related to the properties of the fibers joined and is referred to as intrinsic (to the fibers) splice loss. Intrinsic parameters include variations in fiber diameter (both core and cladding), index profile (α and Δ mismatch), and ellipticity and concentricity of the fiber cores.

EXTRINSIC SPLICE LOSS FACTORS

- TRANSVERSE OFFSET
- LONGITUDINAL OFFSET
- AXIAL TILT
- FIBER END QUALITY

INTRINSIC SPLICE LOSS FACTORS

- FIBER DIAMETER VARIATION
- α MISMATCH
- Δ MISMATCH
- ELLIPTICITY AND CONCENTRICITY OF FIBER CORE

FIGURE 8 - Intrinsic and Extrinsic Splice-Loss Factors

A number of analytical models have been developed to

determine the effect the various intrinsic and extrinsic parameters have on splice loss. Fig. 10 compares the relative influence on splice loss of the major extrinsic parameters of transverse offset, end separation, and axial tilt, for multimode graded-index fibers. Splice loss is significantly more sensitive to transverse offset and axial tilt than it is to longitudinal offset. For example, a transverse offset of 0.14 core radii or an axial tilt of 1 degree (for a fiber with an NA = 0.20) will produce a splice loss of 0.25 dB. A longitudinal offset of one core radius will produce a loss of only 0.14 dB.

A matching material with a refractive index approximately the same as that of the core is used to reduce the Fresnel reflection loss caused by the glass-air interfaces between the coupled fibers of a joint.

The mismatch of intrinsic multimode graded-index fiber parameters can also significantly affect the loss of a splice. Fig. 11 illustrates how splice loss is affected by core radius or Δ mismatch and Fig. 12 shows how it is affected by α mismatch. These curves were obtained using a model in which a gaussian distribution of the power within the solid angle defined by the local numerical aperture at any point on the fiber core was assumed. Sensitivity of splice loss to mismatch is therefore substantially less than that for Δ or core-radius mismatch. Although generally less significant, other intrinsic mismatch parameters, such as core ellipticity and concentricity, do contribute to the total loss of a splice.

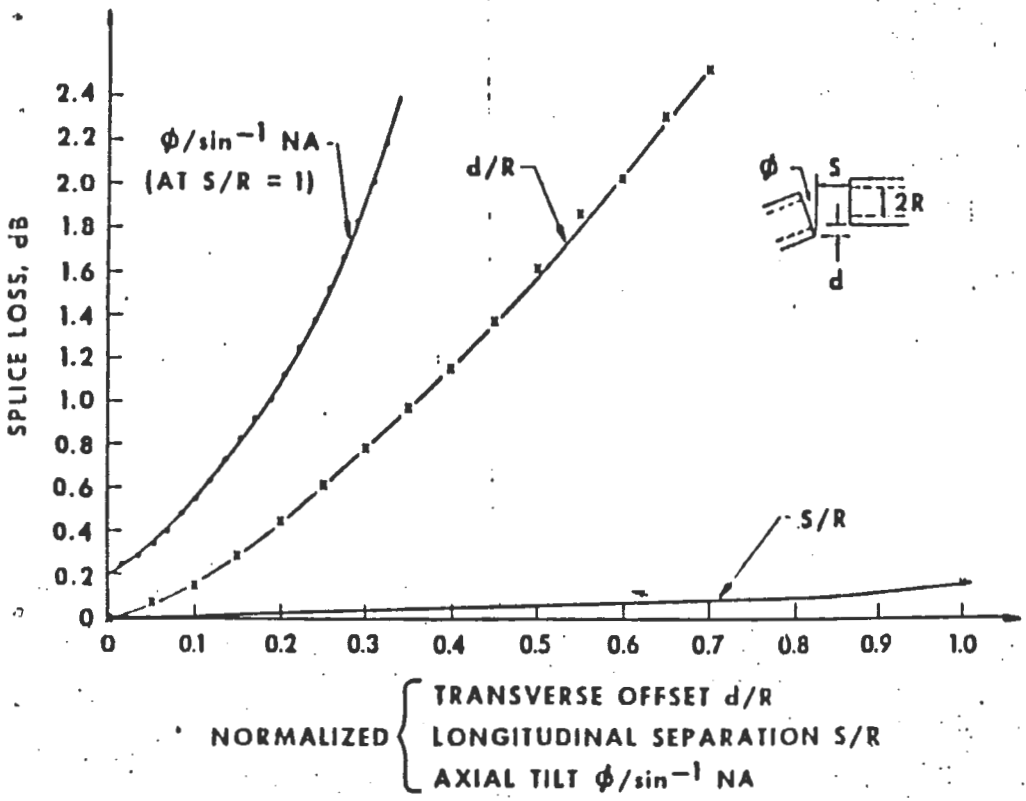

FIG. 10 - Splice loss due to extrinsic parameters.

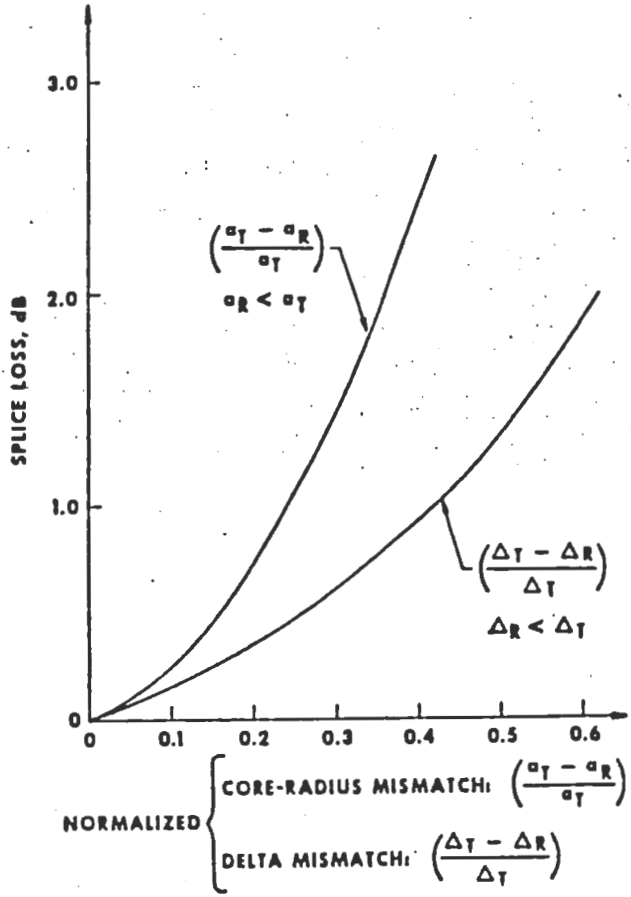

FIG. 11 - Splice loss due to core radius and delta mismatch.

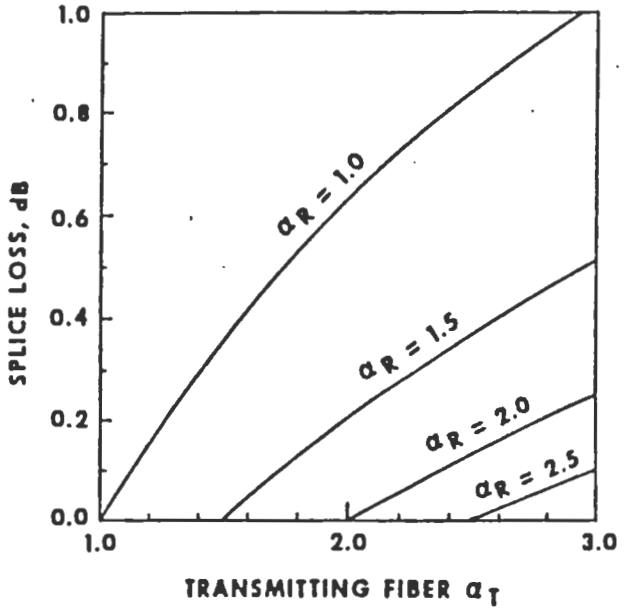

FIG. 12 - Splice loss due to α mismatch.

In summary, the most important extrinsic parameters that cause loss are transverse offset and axial tilt. One must carefully design both connectors and splices to very tight tolerances to minimize these extrinsic parameters. The most sensitive intrinsic factors that cause splice loss are the Δ and core-radius mismatch of the fibers being joined. To minimize the effect intrinsic parameters have on splice loss, tight manufacturing tolerances on the fibers used in a low-loss communication system must be maintained.

SINGLE-MODE SPLICES

The offset loss of single-mode fibers depends on the form of the propagating mode. In both SI and parabolic-index fibers, the beams are nearly Gaussian. The loss between identical fibers is

$$L = -10 \log (\exp - (d/W)^2) \qquad (9)$$

where w is the spot size. For SI fibers operating close to a normalized frequency V of 2.405 the spot size is about 1.1 times the core radius. The single-mode axial displacement loss is plotted in Fig. 13. Because the spot size is only a few microns, we realize that efficient coupling of single-mode fibers requires a very high degree of mechanical precision. For a loss of 1 dB, Eq. 9 yields d/w = 0.48. If the spot size is 4 μm, the allowable misalignment is only 1.9 um.

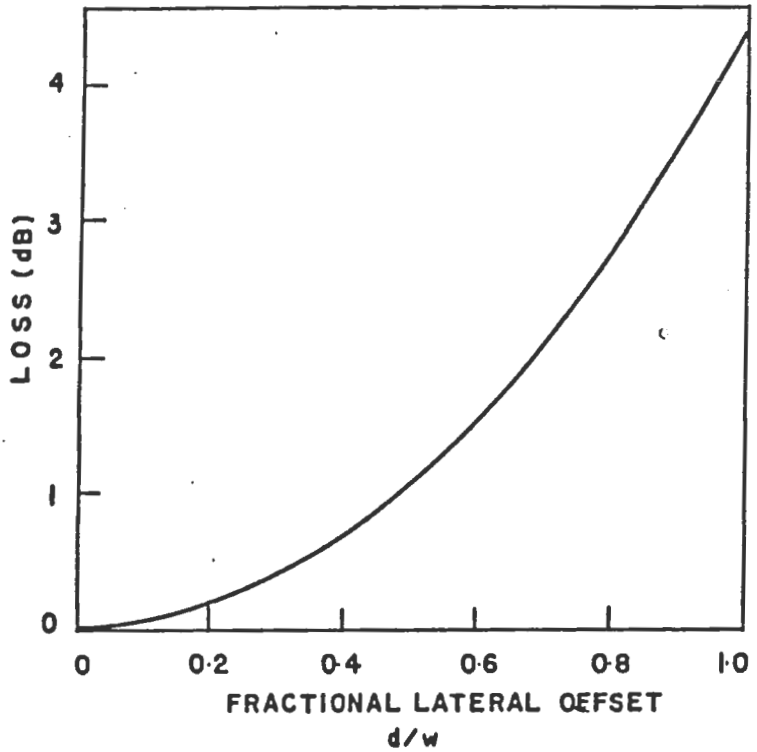

FIG. 13 - Lateral misalignment loss for single-mode fibers whose modal spot size is W.

For single-mode fibers the angular misalignment loss is

$$L = -10 \log (\exp - (\pi n_2 W\theta/\lambda)^2 \qquad (10)$$

where θ is the radians, w is the Gaussian spot size, and n_2 is the refractive index of the cladding. The loss is plotted in Fig.14 for two different SI fibers, both having a normalized frequency of 2.4 and a cladding index of 1.48. As with the multimode case, the loss increases more quickly for the fiber with the smaller numerical aperture.

The gap loss for single-mode fibers is

$$L = -10 \log \frac{4(4z^2 + 1)}{(4z^2 + 2)^2 + 4z} \qquad (11)$$

where $Z = x\lambda/2\pi n_2 W^2$. This result is plotted in Fig. 15 for a fiber having NA = 0.12. For this example, a gap of 10 times the core radius produces a loss less than 0.4 dB. We conclude that the gap is not too critical. As with multimode fibers, axial misalignment is potentially the most serious problem.

INDIVIDUAL-FIBER SPLICES

Individual-fiber splices can use glass capillary tubes to provide robusts, easy-to-handle terminations for individual fibers in much the same way as silicon chips do for multiple fibers.

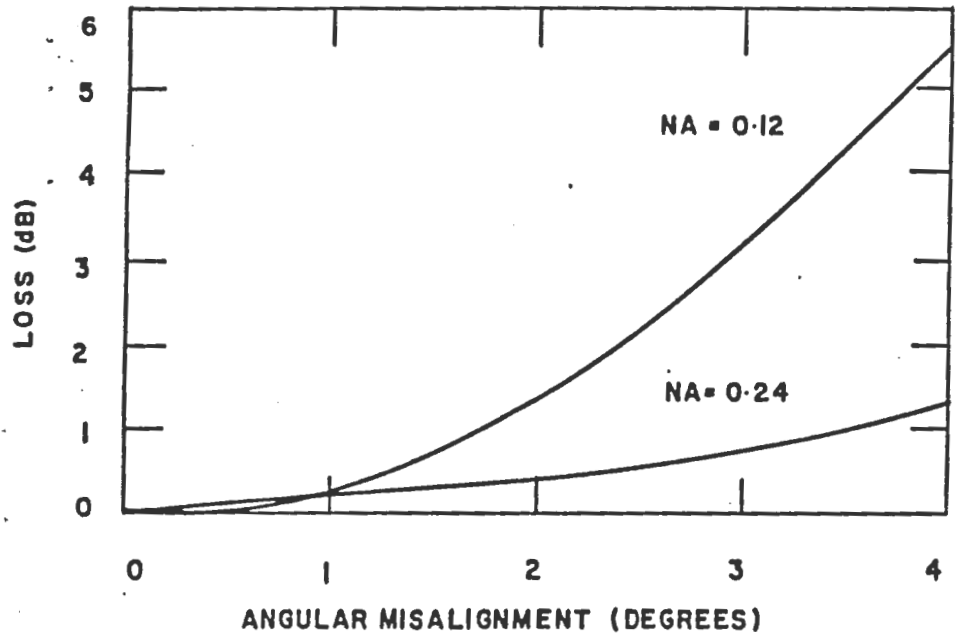

FIG. 14 - Angular misalignment loss for single-mode SI fibers. $V = 2.4$, $W/a = 1.1$, $n_2 = 1.48$, and $\lambda = 0.8\ \mu m$.

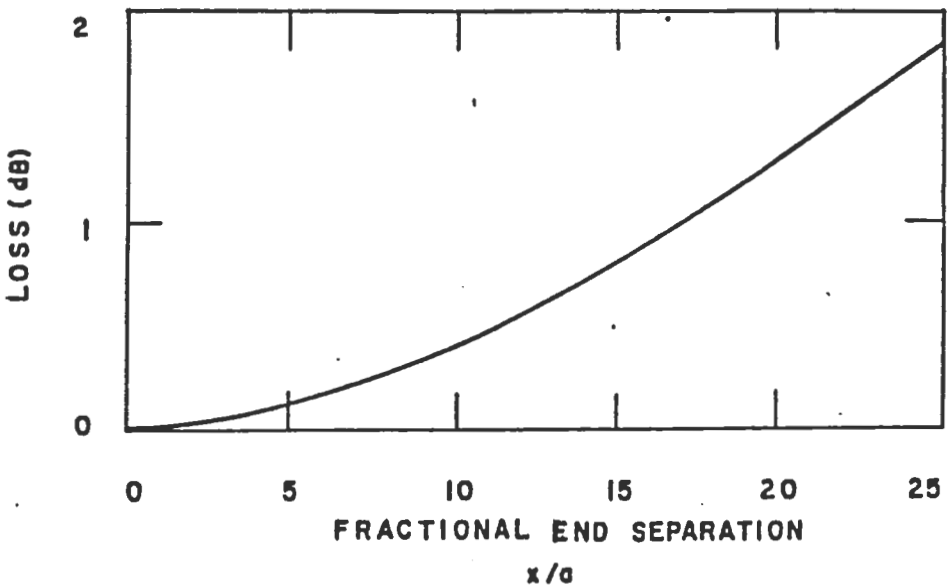

FIG. 15 - End separation loss for a single-mode SI fiber.

$V = 2.4$, $W/a = 1.1$, $n_1 = 1.465$, $n_2 = 1.46$,

$NA = 0.12$, $\lambda = 0.8\ \mu m$.

Accuracies and tolerances of glass tubes combined with careful mechanical design allow MM and SM fibers to be spliced with average splice losses of 0.30 dB without using any test equipment. Active alignments allow tuning of rotary SM splices to less than 0.05 dB even when splicing is done in the field.

The MM mechanical splice was the first glass tube splice. MM fibers are terminated in glass-tube assemblies using ultraviolet-curable cement, and the ends are ground and polished. Each ferrule is inserted in opposite ends of a cylindrical alignment sleeve and index matched with the same gel used with silicon chip arrays. Splice loss average 0.2 dB with no tuning or can be tuned to below 0.1 dB by active alignment. Losses are acceptable for MM fibers but not for SM fibers.

To achieve SM splice losses of 0.05 dB requires core alignment to within 0.4 μm. The rotary mechanical splice consistently achieves such alignment with no precision positioners of any kind.

The principle of operation for the rotary mechanical splice is shown in Fig. 18 . Each fiber is mounted slightly off center in a glass ferrule, and the two ferrules are offset relative to each other so that two positions of perfect alignment are available when the ferrules are rotated. The rotary mechanical splice is manually adjusted to one of these positions without sophisticated positioners.

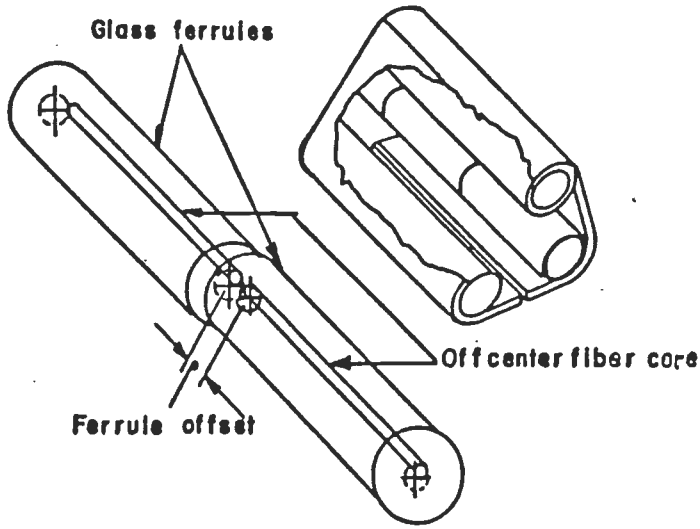

FIG. 16 - Rotary splice and the alignment sleeve for rotary mechanical splice.

Fig. 16 shows the alignment sleeve for the rotary mechanical splice. This sleeve is designed to obtain extremely stable splice loss (0.02 dB variation) over a wide temperature range (- 40° F to + 170° F) with no residual loss. Productivity is typically 10 minutes per splice including termination, tuning, testing, and splice storage.

An enhanced, second-generation rotary splice - called the prealigned rotary (PAR) SM splice - achieves low loss (0.20 dB) without tuning. Splicing procedures and tolerances of the glass tubes have optimized to achieve these results: however, the splice can be optionally tuned to values below 0.05 dB with active alignment. The three largest offset-producing effects in glass-tube SM splices are:

- Eccentricities in the bore of the glass tubes
- Oversize diameter of the bore
- Eccentricities in the core of the fiber.

A second example of a permanent splice that utilizes an alignment member is called a Springroove splice and is shown in Fig. 17 . This splice uses a bracket containing two cylindrical pins as the alignment element (groove) for the fiber ends being spliced. The diameter of the cylindrical pins is selected to ensure that the upper rim of the fibers stays above the cylinders, as shown in Fig. 17b . An elastic element (a spring) is used to keep each fiber end pressed in the groove and a drop of commercial optical epoxy is added to complete the splice. A

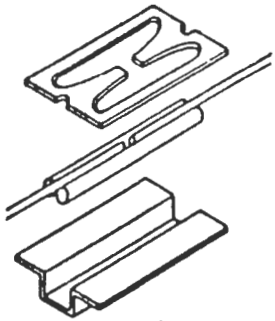

(a) EXPANDED VIEW OF SPRINGROOVE® SPLICE

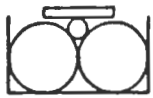

(b) SCHEMATIC OF CROSS SECTION OF SPLICE

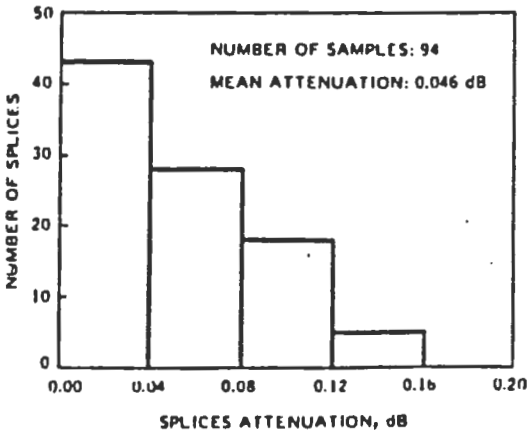

(c) HISTOGRAM OF LABORATORY SPLICE LOSS DATA

FIG. 17 - Springroove splice.

histogram of loss data resulting from laboratory tests performed utilizing Springroove splices is shown in Fig. 17c . The average loss for these laboratory tests using identical multimode graded-index fibers was 0.048 dB.

LOCAL INJECTION DETECTION

Both fusion and mechanical splices often use active alignment to minimize offsets. Although far-end transmission monitoring has been used in the field, it is a cumbersome technique compared to the convenience of local light detection. Local detection can be done by sensing the light transmitted through the splice or sensing the light lost at the splice. The sensitivity of local loss detection is 200 times greater than the sensitivity of local transmission. Because local loss detection equipment can be easily calibrated, accurate splice-loss measurements can also be accomplished with this technique.

There are two fundamental processes used to inject or couple light into the core of a single-mode fiber: microbending and macrobending. These bends couple light from the fundamental LP01 mode to the LP11 leaky mode and vice-versa. Conventionally, light from a 0.8-to 0.9- μm LED source is focused on to a relatively small radius (to 1 to 5 mm) macrobend to inject typically - 50 dBm or less light into the fiber. Although this technique will work satisfactorily with transmission detection,

most fibers are not single-mode at 0.8 to 0.8 μm. Moreover, a large portion of the -50 dBm is sometimes in the cladding; and fiber-to-fiber variation is usually high. These factors combine to yield poor splice alignment and give no indication of splice loss.

Local light injection using short-period, small-amplitude microbends has several advantages:

1. The modulated 1.3-μm laser source excites the single-mode fiber properly.
2. Greater than -35 dBm can be injected almost totally in the core.
3. Bending stresses are less than 50 kpsi.
4. Fiber-to-fiber variation is low.

A schematic of the microbending region itself appears in Fig. 18 .

RAPID RIBBON SPLICING

In the rapid ribbon splicing, all 24 fibers of a splice are ground and polished simultaneously. Then a portion of the ribbon is removed, and the bare fibers are placed into a grooved substrate with the ends butted. The continuous grooves of the substrate align the fibers, and a matching gel is placed between the fiber ends to reduce the splice loss and reflection. A molded cover is placed over the fibers and secured with spring fasteners to retain the alignment. Only simple hand tools, a vacuum pump,

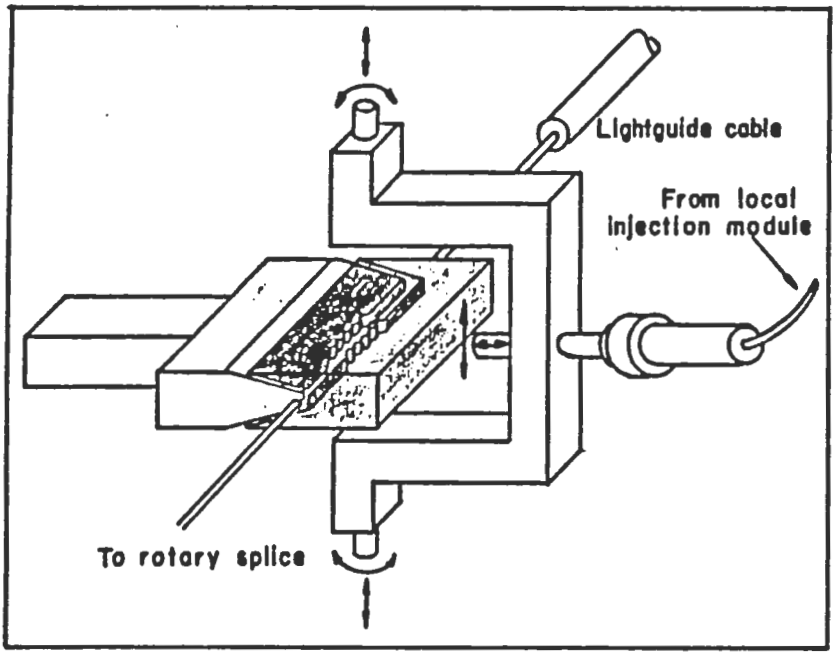

FIG. 18 - Schematic of local injection by microbends.

and a fixture with a low-power microscope are required to make the splice.

Average splice loss is about 0.35 dB with a standard deviation of about 0.3 dB. The splices are very stable: added loss over a temperature cycle from -40 °F to 170 °F is less than 0.05 dB with no residual loss after cycling.

CONNECTORS

Optical fiber connectors are used to couple light from a source to fiber, from one fiber to another, and from fiber to a detector. The first and third are special applications and will not be discussed here.

By far the most popular configuration for optical fiber connectors is the precision-aligned butt joint with ground and polished ends. The fibers are positioned and held in supporting ferrules as the ends are ground and polished. These ferrules, which are usually cylindrical or conical, are then aligned in sleeve couplings (Fig. 18). Good alignment of the fiber cores require precise diameter and concentricity control of the cylindrical ferrule and sleeve, and precise taper length and concentricity control of the conical parts.

Some connectors use an expanded-beam lens, as shown in Fig.18c . This connector has relaxed concentricity requirements but this is offset by more stringent angular requirements. Because the ends can be sealed with glass disks, the connector is less

The molded biconical plug connector shown in Fig. 20 is widely used as part of a jumper cable for a variety of central office applications in the Bell system. The heart of this connector is a biconical sleeve which accepts two plugs and aligns the axes of the fiber ends that are centrally located in these plugs. An inherent advantage of the conical alignment configuration is that virtually no abrasive wear occurs with repeated engagement of the plug and alignment sleeve. No contact occurs between the mating parts until the plug is fully seated within the biconical alignment sleeve. Both the plugs and the alignment sleeves are transfer-molded using a filled thermosetting epoxy to enhance dimensional accuracy and stability. Each plug is molded directly onto a fiber. Careful prepositioning in the transfer mold ensures that the fiber core is concentric within a few micrometers to the tapered end surface of the plug. After molding, the end of the fiber is ground and polished. To complete a connection the two plugs are inserted into the biconical alignmnet sleeve as shown in Fig. 20. The lowest average measured insertion loss obtained with identical 50 μm/125 μm graded-index fibers (NA = 0.23) for this connector was 0.11 dB and 0.2 0.1 dB for single-mode fibers. Fresnel reflection loss can be virtually eliminated in this connector by allowing physical contact of the carefully polished fiber end faces.

The next connector design that we will discuss uses a

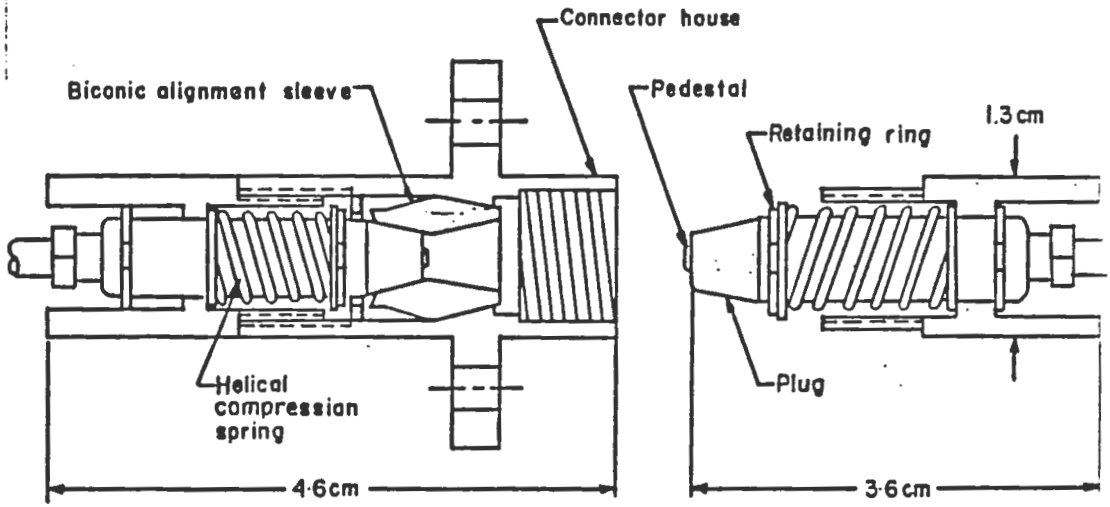

FIG. 20 - Expanded view of a biconical connector.

three-ball alignment configuration to center a fiber in a ferrule arrangement shown in Fig. 21a. The fiber is located in a groove formed by two balls and held in place by a third ball. To ensure correct location of the two fiber ends they are located with a microscope and recessed with respect to the end plane of the three balls. The fibers are then permanently attached with an adhesive. The geometrical characteristics relating the fiber end recess and ball radius are shown in Fig. 21b. By pressing together the two sets of three balls, automatic alignment of the two fibers is brought about. It should be noted that the only high-precision components in this connector are the tungsten carbide balls that are inexpensive and easily manufactured with tolerances of ± 1 μm. Average insertion losses of 0.5 to 1.0 dB have been reported using a 50-μm core-graded-index fiber. A modification of the three-ball connector using fiber bead terminations is shown in Fig 21c. The beads, whose spherical flame-polished surfaces reduce coupling losses due to imperfect fiber cleaving, are produced using an electric arc discharge. An inexpensive molded plastic connector using a three-ball insert and fiber-bead terminations had an average loss of 0.8 dB.

BIBLIOGRAPHY

- J.M.Anderson, D.R.Frey and C.M.Miller, AT&T Technical J., 66 (1), 45 (1987).

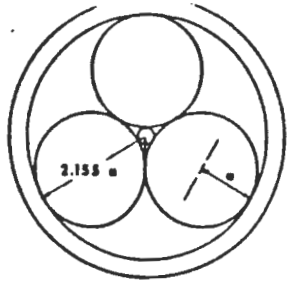

(a) FIBER LOCATED IN GROOVE FORMED BY THREE CONTACTING BALLS

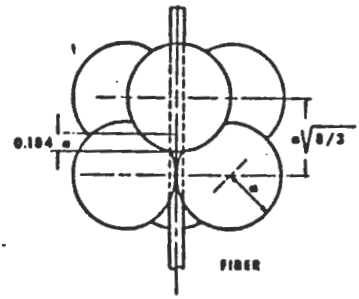

(b) TWO INTERLOCKING, SELF-ALIGNING SETS OF THREE BALLS

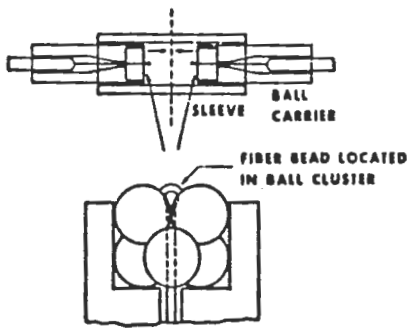

(c) THREE-BALL FIBER-BEAD CONNECTOR

FIG. 21 - Single-fiber three-ball connector.

- A.H.Cherin, "An Introduction to Optical Fibers", Mc Graw Hill Int, London (1983).
- "AMP Designers Guide to Fiber Optics", Ed. AMP Inc, Harrisburg, PA (1982).

BIDIRECTIONAL COUPLERS

INTRODUCTION

To perform some of the basic functions required in any optical system, several in-line optical fiber components were developed, such as polarization controllers, modulators, power dividers, passive filters, and fiber amplifiers. One of the important functions that was first considered was the transfer of signal power between two optical fibers, which is the prerequisite for many interesting applications. Various approaches were investigated by different authors, using either multimode or single mode fibers, which led to several coupler geometries. Some of these approaches rely on evanescent wave coupling, which requires that the fiber cores be brought close enough to each other to make possible the interaction of the evanescent fields which extend just outside of the cores. However, and especially in the case of single mode fibers, the fiber core is rather small and buried inside a 100 μm diameter cladding, so that acess to the guided mode is generally difficult.

Three major techniques of fabrication of fiber-to-fiber couplers have been published to date. Multiport fiber couplers were fabricated using a fusion method. Significant coupling ratios (up to 50 percent) and relatively low loss (0.2 dB) were reported with such couplers using multimode fibers. An etching method has also been published in which two single mode fibers are chemically

etched until most of the fiber cladding is removed. Finally, mechanical polishing has been used to demonstrate efficient coupling.

We present in this lecture an overview of the basic principles on which polished and fused bidirectional couplers operate. Details of the fabrication are given and the experimental results are discussed based on simple theoretical considerations.

POLISHED COUPLER

A schematic of the fiber coupler is shown in Fig. 22 . A length of optical fiber is bonded into a slot in a quartz block with parallel, polished faces. To provide additional mechanical stability during polishing, and to control the length of interaction in the final device, the bottom of the slot is given a convex curvature with a specified radius. The surface of the substrate is first ground, then polished until the desired proximity to the fiber core is obtained. The distance from the substrate top surface is measured either with a low depth of field microscope, with a mechanical instrument or by measuring the axis dimensions of the oval pattern at the intersection of the cladding and the substrate. When enough substrate has been removed, two such substrates are mated to form a coupler, as shown in Fig.22c . Observation of the interference pattern produced within the thin layer of air between the two substrates yields important

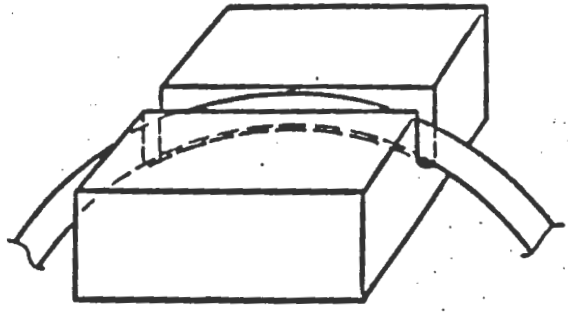

(a)

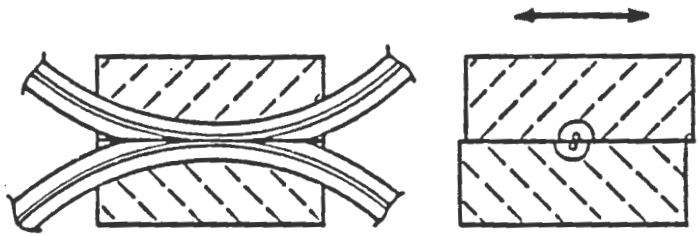

(b)

FIG. 22 - Geometry of the curved-fiber optical coupler showing (a) the position of the fiber in its quartz substrate; (b) a longitudinal and transverse cross-section of the assembled coupler.

informations on the quality of the polished surfaces.

During preliminary tests and routine operations, the coupler is placed in a holder provided with micrometric screws to adjust the position of the top substrate with respect to the bottom substrate (Fig. 23). The purpose of these positioners is twofold: first, to align the fibers parallel and superposed, which can be checked by looking at the oblong cladding patterns of the fibers through the top substrate with a microscope: second, to offset the top fiber with respect to the bottom fiber by any amount.

THEORETICAL MODEL

In the simple case of a single fiber, the wave equation subjected to an appropriate set of boundary conditions can be solved exactly, leading to a good mathematical description of all the fiber modes. When two fiber cores are nearby, as in a fiber coupler, it is more difficult to derive an exact analytical form of the eigenmodes of the system, mainly because of the symmetry breakdown introduced by the presence of a second waveguide.

In order to solve the theoretical problem of a two-waveguide system, an alternate approximate method was developed which uses a perturbation formalism. When two dielectric waveguides are placed alongside each other, the introduction of the second guide distorts the field distribution of the guided mode of the first guide. The approximation consists in assuming

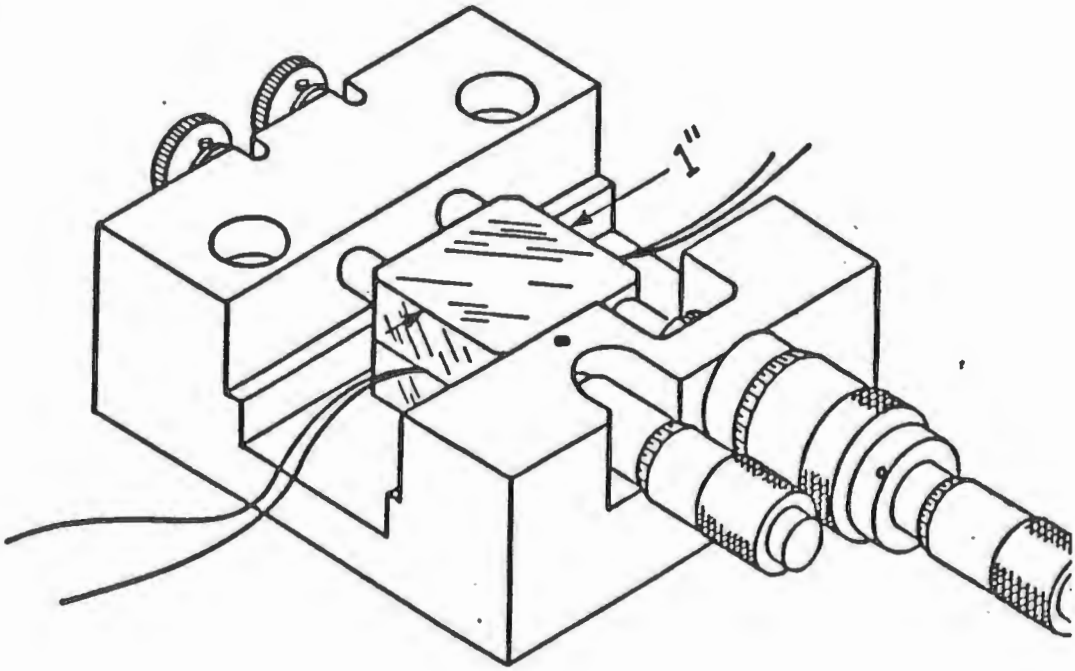

FIG. 23 - General view of a fiber coupler in its holder.

that each waveguide mode distribution remains unperturbed, and in expressing the field of the two-waveguide system as a linear combination of the unperturbed field of each waveguide in which the field coefficients depend on the position z along the direction of propagation. This z-dependence, which accounts for the transfer of electromagnetic energy between the excited waveguides, has been explicitly calculated by several authors. The power distribution after a distance of interaction z inside a lossless coupler consisting of two parallel waveguides is given by

$$P_3 = P_1 \cos^2 (CZ)$$
$$P_4 = P_1 \sin^2 (CZ) \qquad (12)$$

where P_1 is the power launched in waveguide 1 at z = 0, and c is the coupling coefficient for the two couplers modes under consideration. The guided energy is periodically transferred back and forth between the waveguides with a spatial period called the coupling length, equal to $L_c = \pi/2c$. The coupling coefficient is simply given by the spatial overlap of the two interacting waveguide modes

$$C = -\frac{\omega\epsilon_0}{4P_1} \int\int_{-\infty}^{\infty} (n^2-n_2^2)\, E_1^* \cdot E_2 \; dxdy \qquad (13)$$

where $n(x,y)$ is the refractive index profile of the waveguides, n_2 is the refractive index of the surrounding material (cladding or substrate), P_1 is the total power carried by the waveguides, W is the angular frequency of the optical signal and E_1 and E_2 are the electric field distributions of the interacting modes. For the current application, the small numerical apertures of the optical fibers used in our couplers allowed us to assume $\Delta n/n_1 = (n_1 - n_2)/n_1 << 1$ so that Eq. 13 can be solved and

$$c = \frac{\lambda}{2\pi n_1} \frac{u^2}{a^2 V^2} \frac{K_0[v(h/a)]}{K_1^2(v)} \tag{14}$$

where λ is the signal wavelength, n_1 and n_2 are the core and cladding refractive index of the fiber, respectively, a is the fiber core radius, h is the distance between fiber axis and K_1 are the modified Bessel functions of the second kind and of order 1. The parameters u and v are the transverse mode parameters and satisfy $u^2 + v^2 = V^2$ where V is the normalized frequency

$$V = \frac{2\pi a}{\lambda} \sqrt{n_1^2 - n_2^2} \tag{15}$$

In a real fiber coupler the fiber geometry departs from the above conditions because the fibers are both curved along a radius of curvature R, and are also allowed to be translated with respect to each other in a parallel (or nonparallel) manner. As a

first consequence the spacing h between the interacting fibers, and therefore the coupling coefficient c(h), is a function of the position z along the coupling region. This problem of distributed coupling was recently solved following similar approaches. It can be easily shown by direct integration of the coupled power along the z-axis that the solution of the new coupled-wave equations is given by

$$P_3 = P_1 \cos^2 (C_o L)$$
$$P_4 = P_1 \sin^2 (C_o L) \qquad (16)$$

where

$$C_o L = \int_{-\infty}^{\infty} C(Z)\, dz \qquad (17)$$

Here we define the integral as the product $C_0 L$ where C (0) is the value of the coupling coefficient at the center of the coupling region (z = 0) where the spacing between fibers is minimum (Fig. 24) and L is the effective interaction length of the coupler.

With the geometry of this fiber coupler, the spacing h(z) between fiber axis is a function of both the radius of curvature R of the fiber and the lateral fiber offset y,

$$h = \left[(h_o + \frac{z^2}{R})^2 + y^2 \right]^{1/2}$$

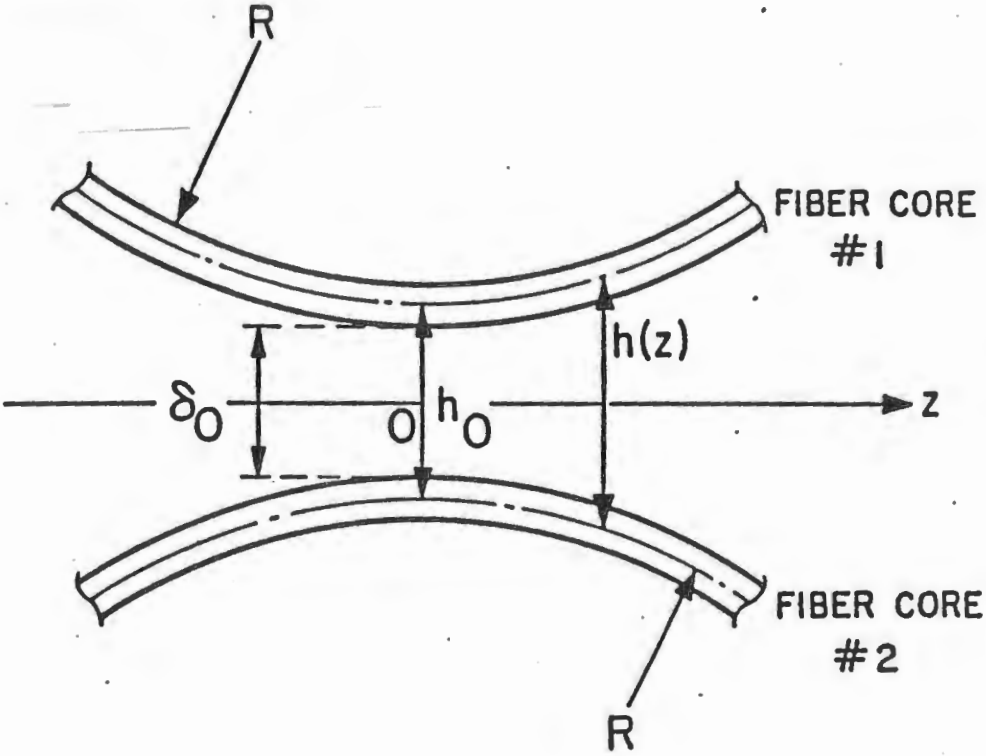

FIG. 24 - Relative position of the fiber cores in the coupling region of a curved-fiber directional coupler. Note that an additional offset (y), perpendicular to the plane of the figure, is also possible.

where a parabolic approximation was used since $z \ll R$.

PRINCIPLE OF WAVELENGTH MULTIPLEXING

The coupling coefficient between two optical waveguides depends on the electric-field distributions of the two waveguide modes involved in the process. Because of waveguide dispersion, these distributions depend on the wavelength of the optical signal. As a result, the coupling coefficient of a waveguide coupler is expected to show some dependence on the wavelength of th injected signal. This effect can be quite significant in single-mode fiber couplers since the HE_{11} modal distribution involved depends rather strongly on the signal wavelength.

This dependence is illustrated in Fig. 25 a , where we have plotted the coupling coefficient vs signal wavelength for different values of the minimum fiber spacing. Figure 25b shows the dependence of the coupling ratio on the wavelength.

Since the coupled power in a single-mode fiber coupler shows a strong dependence on signal wavelength, an interesting application of directional couplers is wavelength multiplexing. In a given fiber coupler with properly chosen geometrical parameters, one signal wavelength can be totally coupled while another remains uncoupled. By feeding the two signals into separate input ports of the coupler, the signals can be mixed and both come out of the same output port. For a given fiber spacing, the coupling lengths

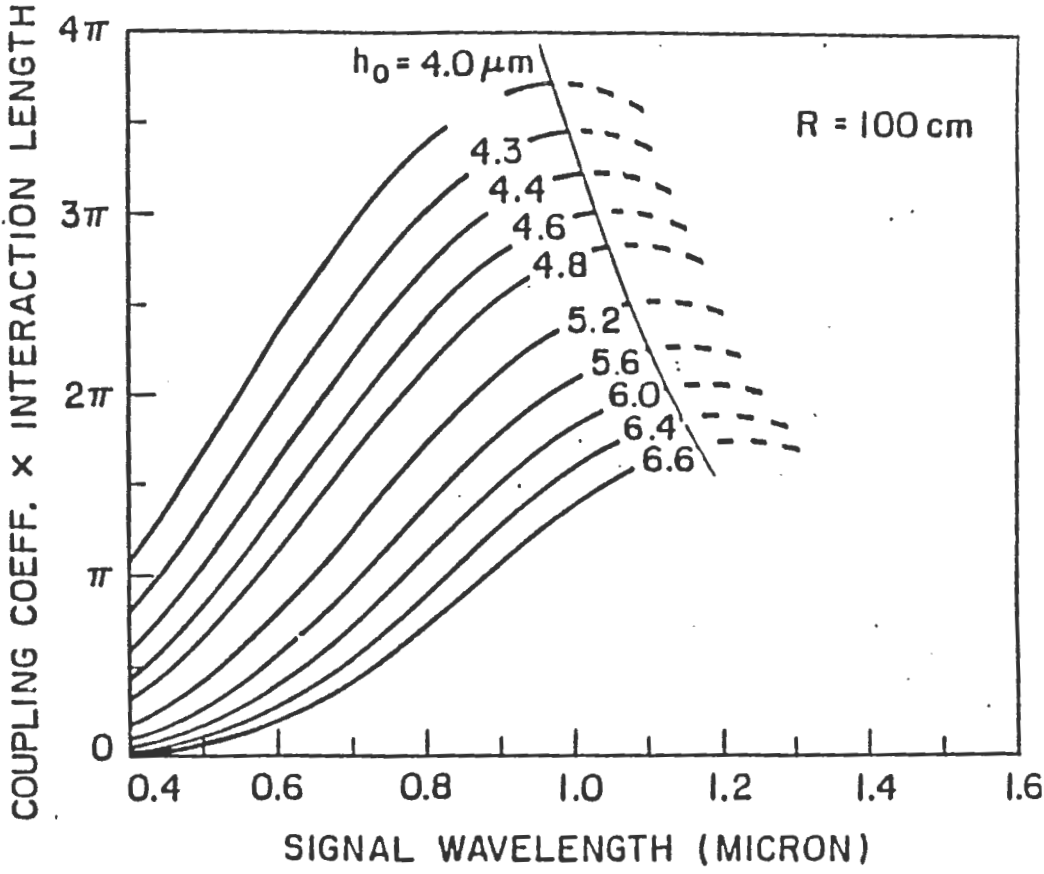

FIG. 25 a - Theorethical dependence of the coupling coefficient of single-mode fiber couplers on signal wavelength for various fiber core spacings.

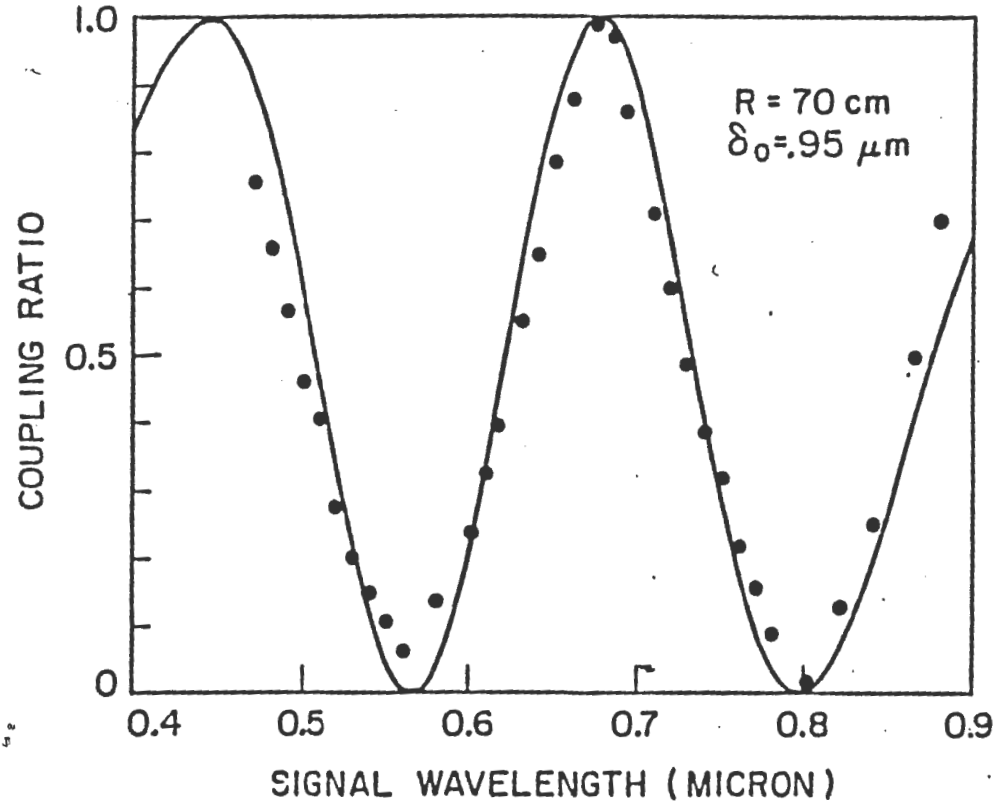

FIG. 25 - Coupling ratio vs signal wavelength in a curved-fiber multiplexer (R = 200cm, δ_0 = 0 μm). An increase in the fiber core offset results in a shift of the coupler response along the frequency range.

for a given pair of signal wavelength are fixed so that the ability of a fiber coupler to mix two signals efficiently depends crucially on the available length of interaction.

EXPERIMENTAL RESULTS

During the fabrication of a coupler, one of the main parameters of interest is the amount of cladding remaining on each substrate. Because the position of the optical fiber in the substrate groove varies slightly from one substrate to the next and cannot be easily measured, the absolute value of n_0 can only be estimated. However, the variation of n_0 between successive polishing operations can be accurately obtained by measuring the variation of the total thickness of the substrate with a microscope or by mechanical means. Figure 28 shows the extinction ratio as a function of remaining cladding for a core-index-matched coupler.

The couplers used for these experiments were polished to different degrees so that they exhibit rather distinct behaviors. If the fiber spacing is made small enough, it is also possible to realize a coupler for which the interaction lengths is longer than the coupling length, making overcoupling possible.

Absolute power loss measurements in curved-fiber couplers were done in two steps. In a first step a relative power loss curve was obtained by measuring the total power transmitted

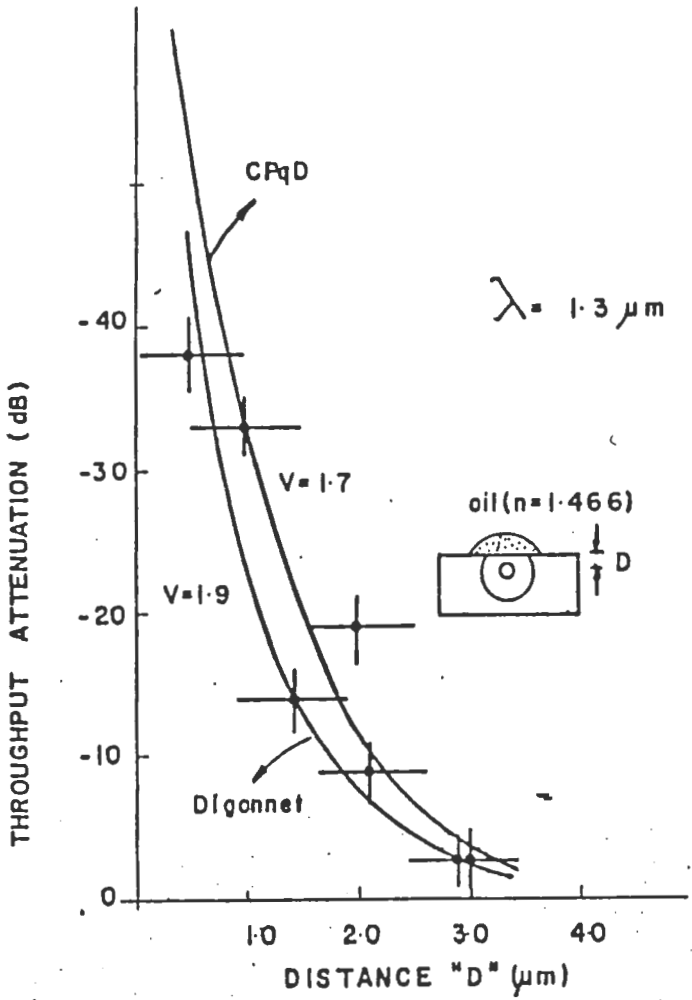

FIG. 28 - Throughput attenuation of a core-index-matched half coupler as a function of removed cladding material.

by the coupler (direct plus coupled power) as a function of the fiber offset. In a second step the power launched into the coupler was measured in a standard manner by cutting the input fiber near its end. This test was found to provide a quick, easy, and accurate means of verifying the quality of a coupler during, as well as after, fabrication.

The spectral loss curve of a typical curve is shown in Fig. 27. In this particular example, the minimum power loss was about 0.3 dB and the coupling ratio was around 0.8 ± 0.1. For fiber offsets larger than 20 μm, the losses somewhat increased because of the decreasing distance between each fiber core and the higher index outer core of the opposite fiber.

Although the above example illustrates the typical power loss of overcouplers, it was found that couplers with large fiber spacings have lower loss levels. In particular, 3 dB couplers may exhibit losses as low as 0.15 dB. Finally, coupler directivity is measured as the ratio of the coupled output to the signal backscattered in the second output fiber. For the purpose of these measurements, the ends of the output fibers have to be either cut at an angle or tapered and dipped in an index-matched liquid to eliminate spurious reflections. Coupling directivity in excess of 50 dB have been reported so far.

CONCLUSION

The SM polishing couplers allow low-loss, quasi-complete

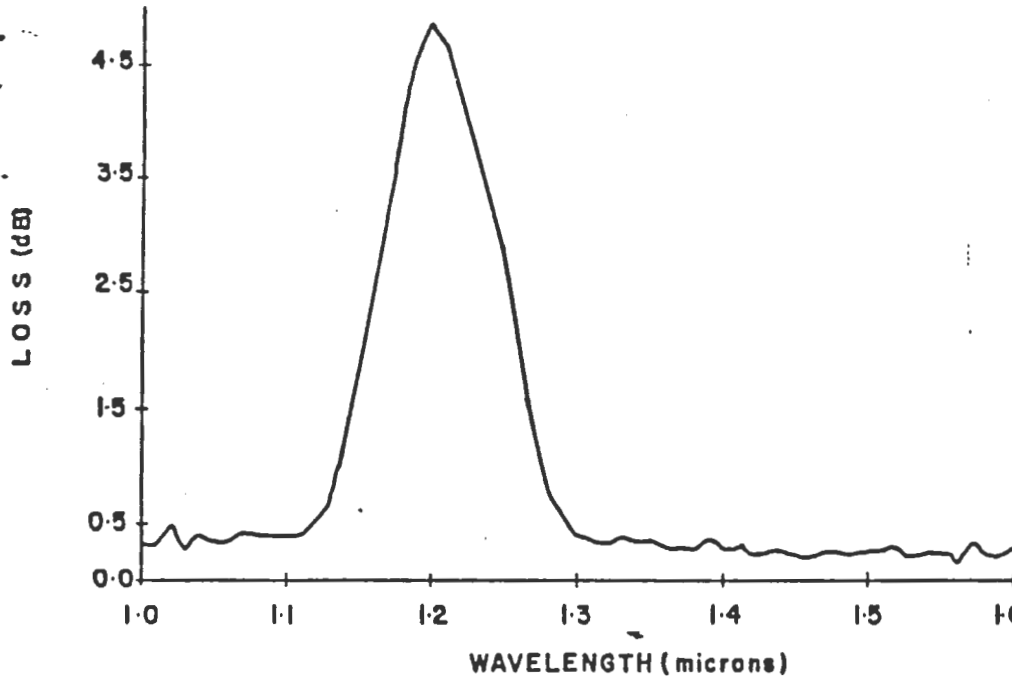

FIG. 27 - Typical spectral loss of a polished SM coupler. The peak centered at 1.2 μm is caused by the cutoff of the LP11 mode.

power transfer as well as operations in an overcoupling regime at different signal wavelengths in the visible and near-infrared range. By controlling the fiber core separation by means of micropositioners, a fine, smooth adjustment of the coupler splitting ratio can be obtained.

FUSED COUPLERS

INTRODUCTION

A multiplicity of coupling device configurations have been proposed, constructed and tested. From a survey of the literature it would seem that optical couplers have been constructed using any conceivable means for processing fiber (cutting, polishing, etching, tapering, splicing and fusing) in combination with a variety of optical components (microlens, reflectors, gratings, graded-index lenses, holograms and thin film waveguides). However, only a few of these many optical-coupler concepts have proven practical and been commercialized. The principal fabrication technique, as attested by the large number of manufacturers who now employ it, is the fuse-pull-and-taper mehod first demonstrated early in 1977 at the Communications Research Centre of Canada. Such couplers in four-port configuration are usually called fused-twin-biconical-taper (FBT) couplers to denote the fact that the geometry of the resultant device derives from a fusion of two fiber bicons tapers to form the coupling region. The attributes that have led to the prominence of FBT technology are:the high performance (low loss, high isolation) of the optical coupler devices made thereby; the fact that devices can be fabricated from a wide variety of fiber types (multimode, single mode, polarization preserving); the

inherent natural compatibility of the optical coupling devices with the optical fibers forming the functional variety of FBT coupler device configurations that are feasible and have been demonstrated. Historically, the first FBT couplers were fabricated from multimode fiber. Although a qualitative description of the operation of the coupler is given here, a comprehensive, detailed theoretical model for the multimode FBT coupler has yet to be developed. Referring to Fig.28 a, light entering port 1 of the FBT coupler propagates into the taper down-region (decreasing transverse device dimension) causing the higher order bound modes to radiate out of the core and be guided as cladding modes. As the waist of the FBT structure, light crosses the boundary between the two fused biconc tapers. The light then passes into the up-tapper region where the cladding modes of the structure are recaptured in proportion to the local cladding mode power by each of the cores of the two output fiber arms of the coupler. This qualitative explanation of FBT coupler operation in terms of the fiber modes may have led to a false conclusion that the fuse-pull-and-taper technique could not be applied to the fabrication of devices made from single-mode fiber, thereby delaying the first demonstration of FBT single-mode couplers until 1981. Even though,the single-mode FBT couplers are fabricated in a very similar way as the multimode FBT couplers,a different model has been proposed to explain the mechanism for power transfer between ports in the single-mode coupler.

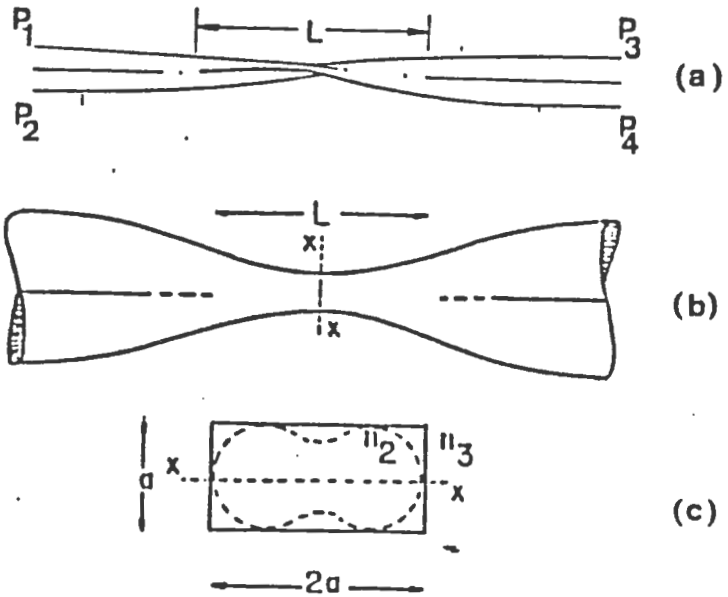

FIG. 28 - Fused biconical taper. (a) The input power P_1 is splitted into the outputs as P_3 and P_4 ; (b) schematic view of the biconical region. L is the interaction length; (c) cross section at the taper waist.

THEORY FOR SINGLE-MODE FBT

The theory of evanescent field coupling, which can adequately describe the behavior of the etched or polished coupler, has been found to be inappropriate when applied to the fused tapered coupler.

The problem with the single-mode tapered coupler is that at some point along the taper, the propagating field becomes detached from the core of the fiber so that in the neck section of the taper the field is guided by the boundary between the cladding and the external medium (i.e. air or some suitable potting material) while the cores are reduced to such an extent that they can be neglected.

Coupling takes place through the interaction of the modes of the composite waveguide formed at the neck section of the coupler by the fusion of the two fibers. Such a model is essential if we are to optimise coupler fabrication and perhaps more importantly if we are exploit fully the modulating and switching capabilities of the fused tapered coupler.

The fused tapered couplers have a structure similar to that of Fig. 28 b .The outer taper angle lies in the range 0.1 - 0.3^{o} . The neck section between the two tapers is approximately parallel with a length up to 2cm. An LP01 mode on an input arm of the coupler is initially guided by the fiber core. On entering the taper section it sees a core of gradually reducing radius. At any point on the fiber the mode can be decomposed locally into plane

waves. This local plane wave decomposition can accurately describe the propagation of the LP01 mode, even for low V-values. The mode will be guided by the core until its local angle of incidence at the core-cladding boundary equals the critical angle. At this point the LP01 mode will refract out of the core and must be considered a field of the entire cross-section of the coupler.

It is postulated that the main coupling action is due to interference between the two lowest-order modes of the section between the tapers, the entire cross-section of which is now considered as a waveguide of refractive index n_2 in a medium n_3. At such large values of V the propagation constants and fields of the two lowest-order modes are insensitive to the detailed shape of the cross-section which can be considered as rectangular dielectric waveguide, as shown in Fig. 28 c .

We considering interference between the lowest-order even and odd modes of the rectangular guide. It is straightforward to derive accurate analytic expressions for the propagation constants of these modes.

If the power of the output ports is described by Eq. 16 then it can be shown that

$$C = \frac{3 \pi \lambda}{32 n_2 a^2} \quad \frac{1}{(1 + 1/V)^2} \tag{18}$$

where V is given by Eq. 15.

In deriving Eq. 18 it is assumed only two modes in the coupling region. If more than two modes were present we would expect to see several periods in the λ dependence.

A more refined analysis for coupling involves integrating Eq. 18 with respect to z along the taper. A further refinement will be to include polarization effects in the coupler. The two orthogonal polarizations have slightly different beat lengths and in very long couplers this results in a modulation of the wavelength dependence. This analysis is presented in the next lecture.

FABRICATION

To prepare to make the coupler, two fibers are stripped of their protective jackets for several centimeters. They are then fixed securely into two opposing translating stages. The fusion process commences with the simultaneous application of heat and tension to the fibers. The heat is removed and the translating stages are stopped when the desired splitting ratio is reached. Both input and output fiber ends are mode-stripped to allow precise measurements to be made. Optimal results require the coupling process to be monitored during the fusion and tapering procedure. A diagram of the essential equipment is shown in Fig. 28 . The particular laser source used is dependent on the desired wavelength of the coupler. 633 nm He-Ne lasers, injection

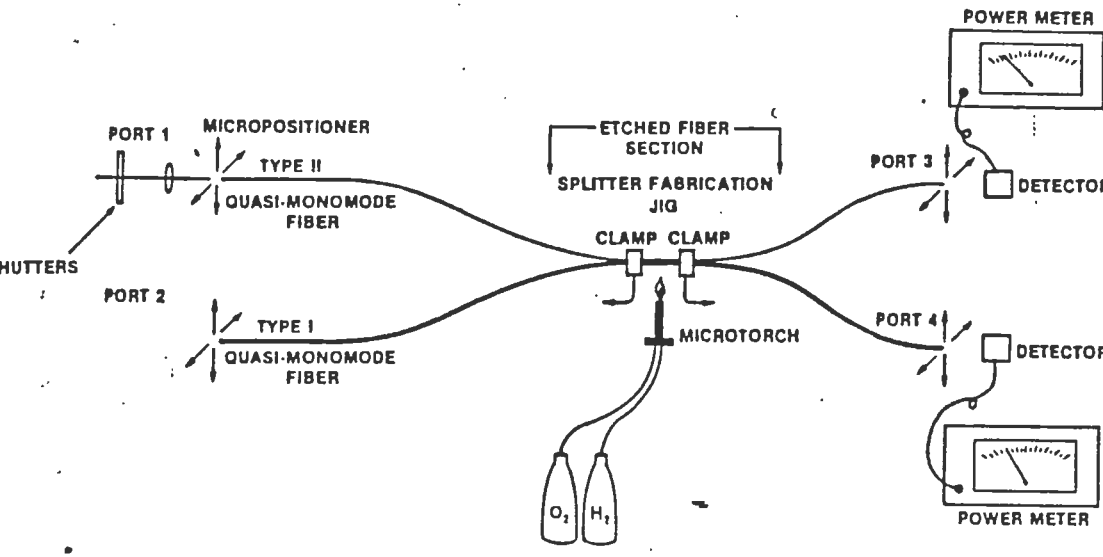

FIG. 28 - Schematic view of a jig for fabrication of fused biconical tapers.

laser diodes of 800 nm and 1300 nm have been successfully employed.

For a SM coupler to be low loss, fiber selection is critical. Efficient coupling requires that the refractive index profile of the fiber not contain a depressed cladding region. Fibers with depressed cladding region prohibit adequate transference of the evanescent field from the input fiber core to the adjacent fiber core.

A measurement of the coupling process was made by recording the optical power of both output ports of a coupler as a function of the length of coupler taper during fabrication. An experimental plot of this data for a particular SM coupler is shown in Fig. 30 . The optical power can be seen to transfer totally from one fiber to the other over a distance, L, commonly known as the coupling length. Coupling ratios between 0 and almost 100% can be obtained by stopping the taper at any point along the curve. The accumulated frequency of the FTB-loss data is presented in Fig. 31. These couplers were fabricated at CPqD/Telebras - BRAZIL.

PACKAGING

The environmental performance of fused biconic taper optical couplers, is strongly a function of the packaging technology used to isolate the glass taper region from mechanical

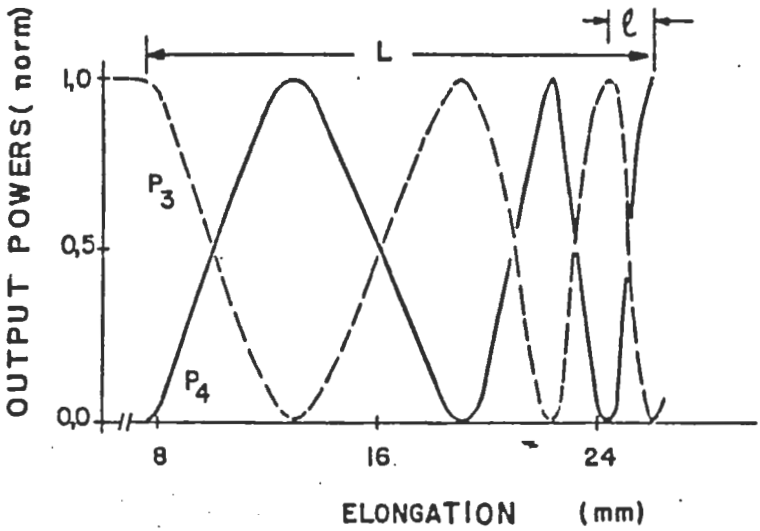

FIG. 30 - Output powers P_3 and P_4 measured during taper fabrication as a function of taper elongation.

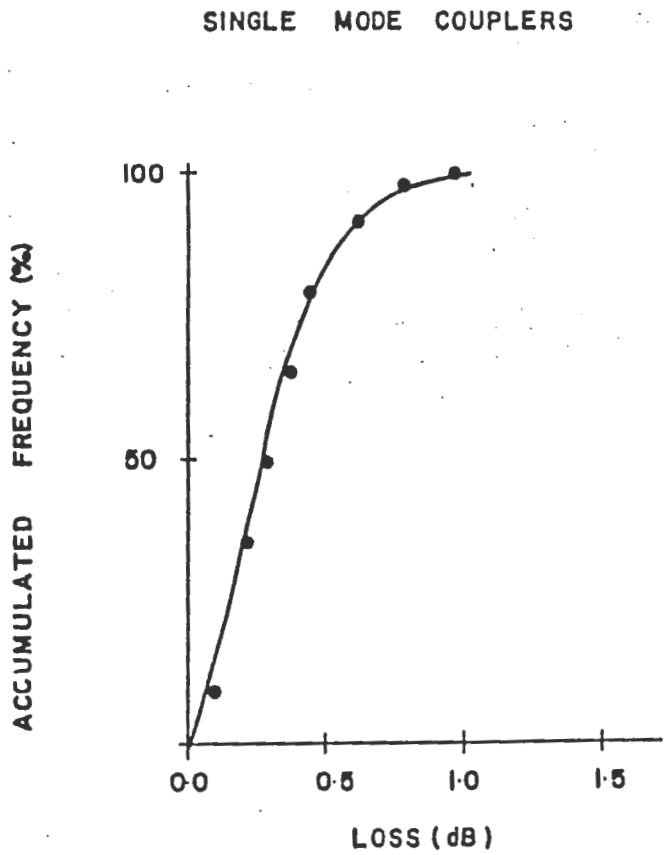

FIG. 31 - Accumulated frequency loss data for fused biconical tapers fabricated by CPqD - Telebrás - BRAZIL.

stress and contamination. Low thermal expansion metals and glasses have been used successfully as substrates in packaging FBT couplers.

Isolating the taper region from mechanical stresses is of primary importance. The minimum taper diameter for large transmission star couplers is on the order of 100 μm. This diameter can measure as small as 12-18 μm for 3 port splitters and combiners using 50/125 μm fiber. The dynamic breaking strength of the taper varies widely because of the handling required to prepare and place the fibers and the heat source used to fuse the fibers. Typically, the dynamic breaking strength is less than 0.5 Newtons (0.1 dB) for 100 μm minimum taper diameters and is correspondingly lower for splitters and combiners. Packaging the taper under zero stress at ambient temperature is accomplished by stress relieving the glass and attaching the fibers to a supporting substrate. To minimize the stress upon the taper at temperatures other than ambient, the coefficient of thermal expansion (CTE) of the substrate must closely match the CTE ofthe glass.

The package configuration is designed to facilitate the manufacturing of couplers. Because the fiber taper region cannot be disturbed, the preferred design was an open ended trough that could be moved into position around the taper for bonding with

adhesive. An oblique view of the package base and lit commercialized by Phaio/DCC is shown in Fig. 32 a. Fig. 32 b shows a top plan view of an assembled coupler with the lid removed. Shown is the placement of adhesive (A) to secure the fibers and adhesive (B) which secures the protective PVC jackets (C) and seals the package ends. The PVC jackets provide bending strain relief for the fibers as they exit the package. The package provides protection against tensile pull out for loads up to 0.5 kg.

BIBLIOGRAPHY

- M.F.J.Digonett and H.J.Shew, J.Quantum Elect., vol. QE-18 (4), 746 (1982).
- M.F.J.Digonnet and J.Shaw, Appl. Opt. 22 (3), 484 (1983).
- Proc. of SPIE, vol. 574, "Fiber Optic Couplers, Connectors and Splice Technology II", David W. Stowe, editor (1985).
- F.P.Payne, C.D.Hussey and M.S.Yataki, Elect.Lett. 21 (11), 462 (1985).
- H.Monteiro, S.Celaschi and J.T.Jesus, CPqD, Rev. Telebras, Sept. 1987, pp. 28 and Rev. Telebras, Dec. 1985, pp. 3.

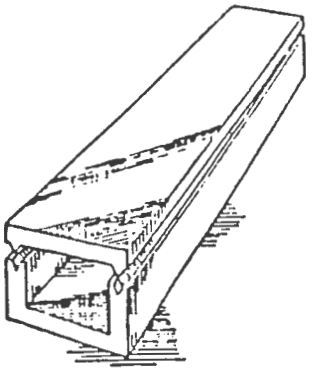

a

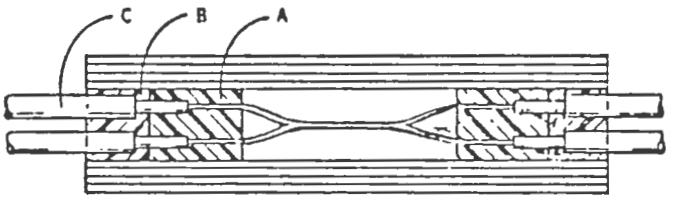

b

FIG. 32 - Package structure of a fused biconical taper commercialized by PHALO.

ALL FIBER TUNABLE LIGHT SPLITTERS AND ATTENUATORS

INTRODUCTION

The rapidly developing applications of single mode fibers in communications have begun to produce tangible demands for couplers and related devices such as tunable beam splitters and multiplexers. These devices may be built from discrete optical components such as microlenses, prisms, beam splitters besides many others. Unfortunately, devices made from discrete components in general present low mechanical stability and therefore are not reliable. Any technique of manufacturing reliable devices should discart discrete components, and should rely only on the fibers and their required packaging structures.

Devices formed using the fused biconical technique find a large variety of uses. The most obvious and simplest example is the fixed-ratio power splitter or directional coupler. Such devices are fabricated as a matter of routine with excess losses of less than 0.1 dB and may be of any desired splitting ratio. A second widely reported application of fused biconical taper couplers is as wavelength-division multiplexers or demultiplexers whereby the wavelength dependence of the coupling ratio of such devices is utilized to mix or separate signals carried at different wavelengths. Variable splitting-ratio couplers have, until recently, been most often of the mechanically tunable polished type. These couplers are in general bulky and their

manufacture requires high precision and is therefore time consuming and expensive.

Electrically controlled all-fibre switches can be fabricated using either of two methods described here. Such devices incorporates the stability, compactness and low cost of biconical fused couplers. Switching has been achieved utilising both the thermo-optic effect, in which a temperature change over a length of fibre introduces bulk refractive index and dimensional changes, and the stress-optic effect, in which the coupler itself is elastically stretched.

MACH-ZEHNDER INTERFEROMETERS

All fibre Mach-Zehnder interferometers for operation at a specific wavelength are conventionally fabricated by splicing two discrete couplers in series. The resulting devices suffer from intensity instability introduced by environmentally induced differential phase changes between the arms.

Recently, it has been showed by Shipley that the consecutive fabrication of 3 dB couplers on two continuous single-mode fibres results in all-fibre MZI which exhibits a stable output intensity even with varying environmental conditions.

The first coupler can be fabricated as a matter of routine using the fused biconical method and by using power monitoring feedback to control the process and achieve a splitting

ratio of 1:1. On the other hand, power monitoring feedback becomes troublesome during the fabrication of the second coupler. To overcome this, an automated coupler production jig can be used to reproduce exactly the fabrication conditions experienced by the first coupler. The completed Mach-Zehnder interferometer is then bonded with UV-curing epoxy to a silica substrate that provides strain relief and mechanical stability to the fused region.

The use of all-fibre MZIs as electrically activated tunable couplers or switches requires the addition of an element to convert an electrical signal into an optical phase shift in the fibre. A method of achieving such electrically controlled optical phase shift can be based on the thermo-optic effect.

THERMO-OPTIC PHASE SHIFTER

A thermo-optic phase shifter can be created by coating each arm of an interferometer with a resistive ink (Fig.33). Wire electrodes connected to the ends of the coated region of one arm provide the link to the external power source. With the application of a voltage across the resistive material the temperature of the fibre arm is raised owing to ohmic heating. The refractive index and dimensional changes hence induced in the fibre result in a different phase shift in the light propagating in the two arms.

The differential phase shift $d\emptyset/LdT$ per unit length

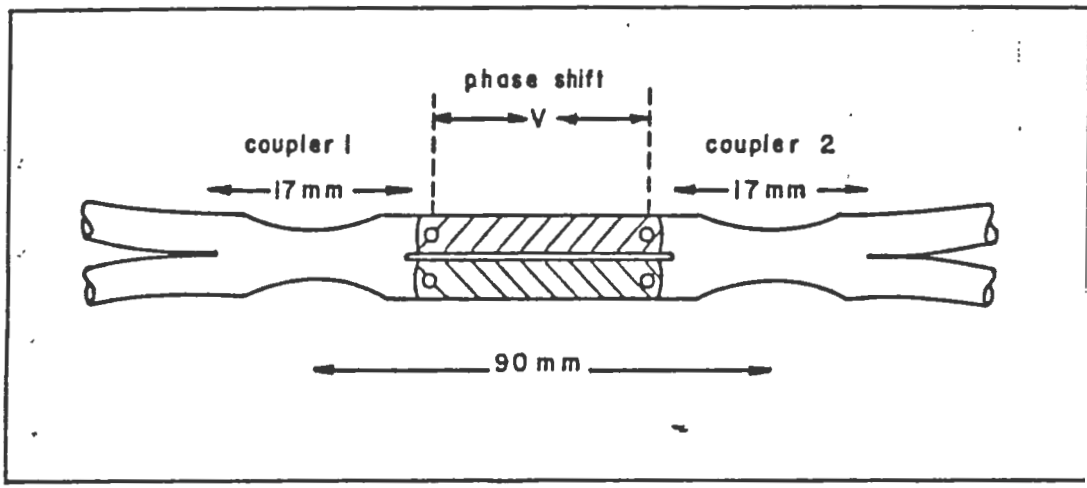

FIG. 33 - Schematic diagram of an all fiber light splitter based on the thermo-optic effect.

induced by temperature change is given by

$$\frac{d\phi}{LdT} = k \left(\frac{n}{L} \frac{dL}{dT} + \frac{dn}{dT} \right) \tag{19}$$

where n is the refractive index of the fibre core, L is the length of the resistively coated region and k is the free-space propagation constant of the light. For pure silica at 1.3 μm wavelength, $d\phi/LdT$ = 40 rad/^{o}C.m. For the microheater reported by Shipley, a phase shift of π radians was predicted for a temperature change of approximately 5°C.

The output power from one arm of the MZI is shown in Fig. 34 as the applied voltage to the thermo-optic phase shifter is varied. A good approximation to this experimental curve is obtained by fitting the following equation to the results

$$P_o = P_i \cos^2 \left(\frac{\pi}{2} \frac{P}{P_\pi} \right) \tag{20}$$

where P_o and P_i are the output and input power, respectively, and P_π is the electric power required for a phase shift of π. $P = V^2/R$, V is the applied voltage and R is the heater resistance. For this particular device, P_π is 25 mW and R = 0.35 ohms.

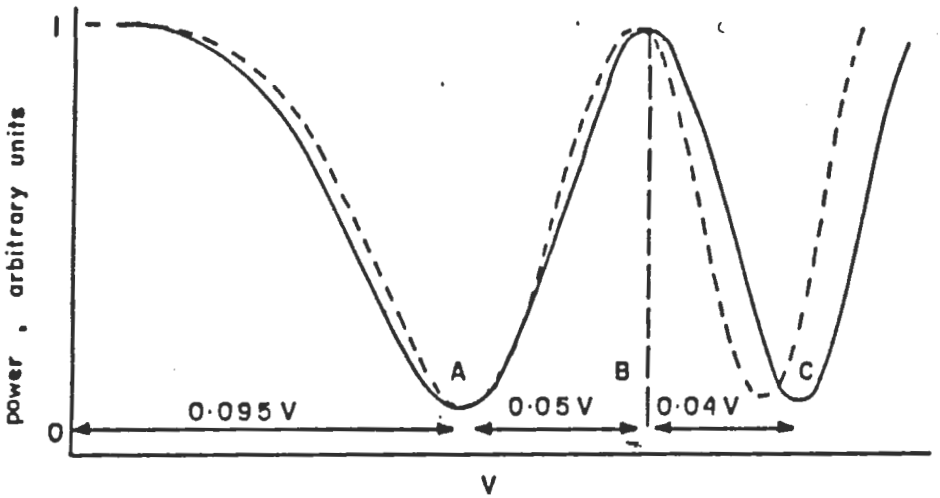

FIG. 34 - Optical power output from one arm of the thermo-optic light splitter.

STRETCHED TAPER AS A TUNABLE LIGHT SPLITTER

The device described herein was fabricated in a manner similar to the fused single-mode couplers which have been reported elsewhere. In review, fused couplers are constructed by bringing together and fusing and tapering a central section of a fiber pair. As the coupler is fabricated, the output intensities P_3 and P_4 are monitored. The process of tapering is interrupted when the desired coupling ratio $r = P_3/(P_4+P_3)$ is obtained. As tapering process continues, the output power is observed to switch sinusoidally from one output power to the other as shown in Fig.35 The coupler is said to have been pulled through one coupling length when the coupled power has switched from the maximum transmitted by one output fiber to the maximum transmitted by the other.

The fused fiber pair constitute a tapered waveguide which differs in two fundamental ways from the monomode waveguides leading into and away from it. Firstly, the fusion and tapering of two monomode fibers produce a highly multimode waveguide owing to the effective sillimination of the original cores, and to the fact that the wave fields are bound by the vastly larger index discontinuity between the glass and the air surrounding the coupler. Secondly, the original cylindrical symmetry is reduced by the necessity to distinguish the transverse direction in the plane of the fused pair from the perpendicular direction. It is the second aspect of the coupling region which permits an

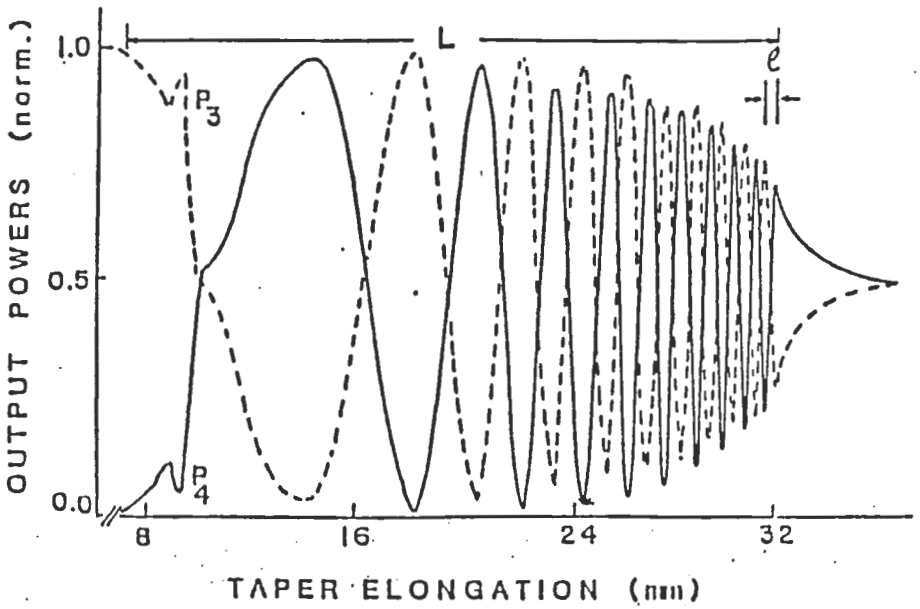

FIG. 35 - Behavior of the output powers P_3 and P_4 during the tapering process. Final dimensions are L = 28mm and ℓ = 0.45mm as defined in text. The total insertion loss is approximately 0.1 dB.

understanding of the observed behavior of the spatial switch.

In the coupling region the traveling wave configuration is the superposition of equal amounts of symmetric and antisymmetric modes, each with a component polarised in the plane of the fiber pair and another perpendicular to it. A small difference between the propagation velocity of the symmetric and that of the antisymmetric modes causes constructive interference to recur alternately on one side and the other along the waveguide, as shown schematically in Fig. 38a . Thus, one of the downstream monomode fibers will transmit a fraction of the normalized input power being its complement transmitted by the other. The transitions between the input and output fibers to and from the fused-cladding composite waveguide occur approximately in regions where the normalized frequency of the tapered fibers approach the unit. This defines the length L of the coupling region. The transition fiber → composite waveguide → fiber are so gradual that little power is radiated, and so, the device is low loss.

In addition, an even smaller difference between the propagation velocity of the x-waves polarized in the plane of the fiber pair and that of the y-waves polarized in the perpendicular direction gives rise in long tapers to a slow amplitude modulation of the high spatial frequency mode beating variations shown in Fig. 35 . Potentially, there are many applications which can

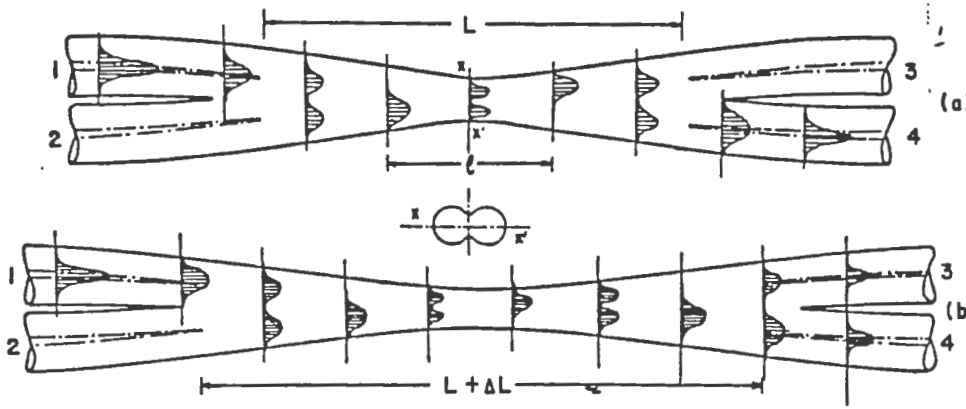

FIG. 38 - Pictorial view of the biconical structure. (a) Without load the interaction length L, and the beating length are defined: (b) the structure is stressed in such a way that $L = \ell/2$.

exploit these properties of long fused couplers. They include polarization beam splitters, spectral filters, modulators and switching, the last being the theme of this paper.

For short tapers such that the interaction length L is only a few times the coupling length ℓ the coupling ratio $r = P_4/(P_4 + P_3)$ is simply given by

$$r = \sin^2 (CL) \tag{21}$$

where C is the coupling coefficient. On the other hand, if the taper is long, it becomes necessary to take into account the small dependence of the coupling coefficient on the polarization direction. For $L \gg \ell$, the coupling ratio is given by

$$r = \frac{1}{2} (\sin^2 C_x L + \sin^2 C_y L) \tag{22}$$

where C_x and C_y are the coupling coefficients in the x- and y-directions respectively.

Thus, r can be modified by axially stressing the taper in such a way that $\Delta L/L = S/Y$ where Y is the Young Modulus for silica, and S the applied stress. The effect of an applied stress on the output powers is schematized in Fig. 38 b for $L = \ell/2$. Fig. 37 shows the variation of the coupling ratio with the applied force F for three different wavelengths. Its sinusoidal dependence on F is

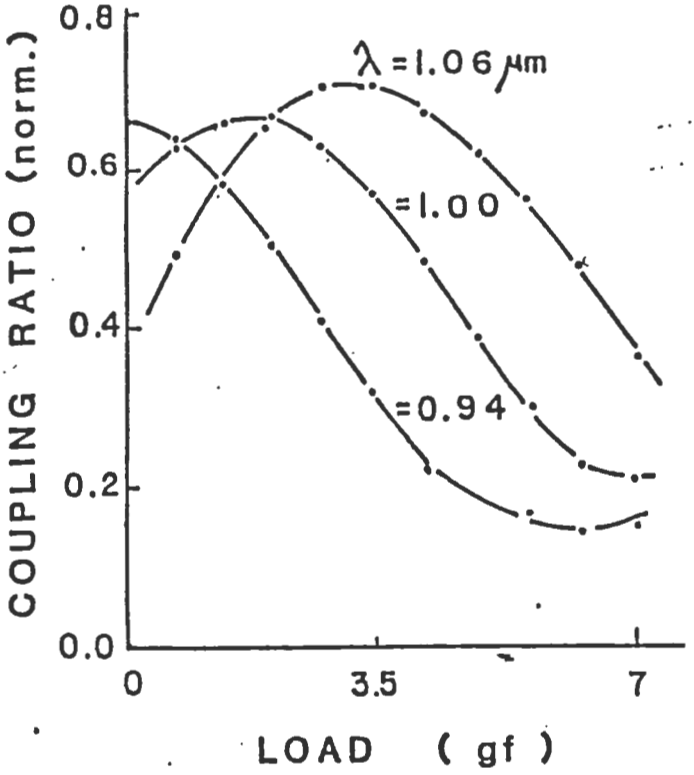

FIG. 37 - Dependence of the coupling ratio on axial stress for three different wavelengths.

explained by the beating model presented above, assuming elastic deformations of the taper structure. One observes in Fig. 38 that the variation in the coupling ratio r is limited to approximately 55%, not reaching complete power transfering as would be desired. This occurs because the tapering process was interrupted before reaching the first complete dephasing of $C_x L$ and $C_y L$. Continuing the tapering process beyond this point, the output powers recover the full sinusoidal amplitude as predicted by Eq. 22 and demonstrated experimentally.

In order to quantify the hypothesis that elastic deformations induce optical beating, we estimated the elongation necessary to cycle the coupled power through one complete sinusoidal oscillation, compering it to that measured experimentally during the final tapering. According to Fig. 37, 7.0 ± 0.5 gf cycles the coupled power through one cycle, which from Hooke Law gives $\Delta L/L = 0.013 \pm 0.004$ for $Y(SiO2) = (10 \pm 1) \times 10^{11}$ dynes/cm^2. On the other hand, one observes in Fig. 35 that the final taper structure has a normalized coupling length $\ell/L = 0.016 \pm 0.003$ in agreement with the estimated strain obtained from the elastic assumption.

In conclusion, we presented in this lecture two simple mechanisms to induce tunable optical d.c. switch, at low losses, on all fiber devices. The conceptual simplicity of these devices make them attractive for operation in single-mode fiber networks.

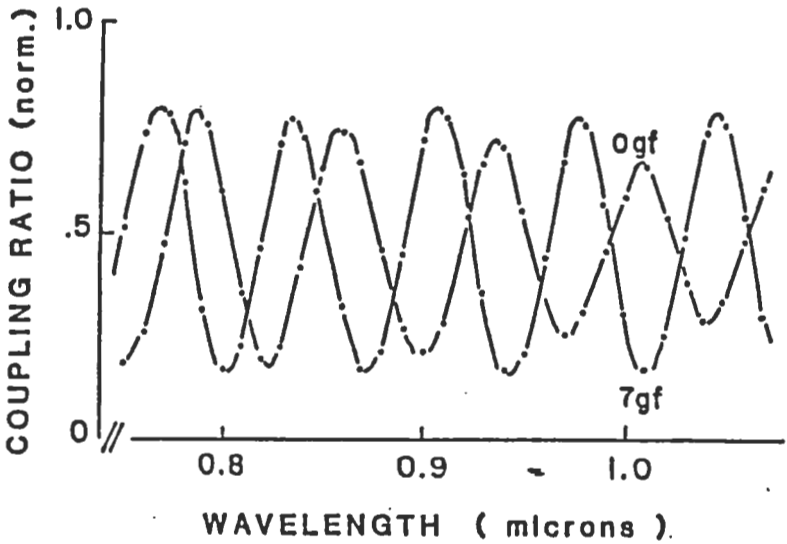

FIG. 38 - Dependence of the coupling ratio of the transmitted wavelength for the unloaded taper and for the taper submitted to 7 gf.

BIBLIOGRAPHY

- S.P.Shipley, G. Georgiou and A.C.Boucouvalas, IEE Proc.; vol. 134, pt. J., nº 3, 203 (1987).

- S.Celaschi, J.T.Jesus and F.M.Smolka, Proc. CLEO/1988.